Developmental effects of polystyrene nanoparticles in the chicken embryo

Wang, M.

Chapter 4. Nanoplastics passive target neural crest cells in the chicken embryo

Meiru Wang[1,2], Carmen L. de Mooij[1], Gerda E.M. Lamers[1], Merijn A.G. de Bakker[1], Martina G. Vijver[3], Michael K. Richardson[1].*

1. Institute of Biology, Leiden University, Sylvius Laboratory, Sylviusweg 72, 2333 BE, Leiden, The Netherlands.
2. Naturalis Biodiversity Center, Darwinweg 2, 2333 CR, Leiden, The Netherlands.
3. Institute of Environmental Sciences, Leiden University (CML), Van Steenis Building, Einsteinweg 2, 2333 CC, Leiden, The Netherlands.

This chapter has been published as part of: Wang, M., Rücklin, M., Poelmann, R.E., de Mooij, C.L., Fokkema, M., Lamers, G.E.M., de Bakker, M.A.G., Chin, E., Bakos, L.J., Marone, F., Wisse, B.J., de Ruiter, M.C., Cheng, S., Nurhidayat, L., Vijver, M.G., Richardson, M.K. Nanoplastics causes extensive congenital malformations during embryonic development by passively targeting neural crest cells. *Environment International* **173**, 107865. https://doi.org/10.1016/j.envint.2023.107865.

Abstract

Plastic pollution is a major environmental concern. Plastics waste in the environment continuously degrades into microplastics and nanoplastics. It has been previously reported that polystyrene nanoparticles can cause neural tube defects in the developing chick embryos. The authors of that study suggested a mechanism whereby nanoplastics cause caveolae-mediated endocytosis in neural tube cells. In Chapters 2 and 3, we found that nanoplastics also cause defects in the eyes, tailbud, heart and vascular system of chicken embryos. However, the mechanism previously proposed, of neural tube damage, could not account for this wide spectrum of malformations. Therefore, in this Chapter, we look in more detail at the cellular mechanisms involved. We exposed stage 8 chicken embryos to 25 nm fluorescent polystyrene nanoparticles in ovo. We found that the nanoparticles became localized to cell masses in the dorsal middle line of the neural tube. Molecular markers identified these cell masses as neural crest cells that had failed to migrate to the periphery. TUNEL staining of nanoplastic-exposed embryos showed that nanoplastics caused death and impaired migration of those cells. When we added fluorescent 25 nm fluorescent polystyrene nanoparticles to primary chick neural crest cells, we found that they could enter the cells within 2 h. Further supporting our hypothesis that nanoplastics specifically disrupt neural crest development, most of the malformations seen in Chapter 2 and Chapter 3 are in organs that depend for their normal development on neural crest cells. Our results demonstrate that polystyrene nanoparticles cause developmental toxicity to chick embryos. Our findings suggest that nanoplastics may pose a health risk to the developing embryo. This is a matter of concern given the large and growing burden of nanoplastics in the environment, and the potential use of nanoplastics in human medicine as drug-delivery vehicles.

Introduction

Plastic as a material is widely used, because of its low cost and ease of production, its versatility and imperviousness to water (Copp et al., 2003). The other advantages of using plastics including high strength-to-weight ratio, ductility, corrosion resistance, bio-inertness, high thermal/electrical insulation and outstanding durability at a relatively low lifetime cost. For these reasons, plastics have enabled progression and changes in a variety of industries, from automotive and aerospace applications, right through to textiles and consumer products, construction and agriculture, and food packaging (Andrady et al., 2015). Its ability to guard against contamination makes plastic useful for example in sterile medical environments such as hospitals, or as food packaging. Nanoplastics are also being considered for therapeutic use in humans, including as drug-delivery systems (Boehnke et al., 2022). Its success in industry and society combined with the persistence of plastic have resulted in plastic waste and pollution being widespread and ubiquitous in today's environment (Andrady et al., 2015). Thus, there are many opportunities for humans to absorb microplastics and nanoplastics (MPs and NPs) by skin contact, food ingestion and even inhalation (Sana et al., 2020).

In Chapter 2, we showed that 25 nm plain polystyrene nanoplastics could cause neural tube defects in developing chick embryos. In humans, neural tube defects are severe congenital defects with high mortality (in the case of cranial defects), long-term disability and costly surgical repair (Oumer et al., 2021). The causes of neural tube defect can be genetic or non-genetic factors (e.g. lack of folic acid; (Copp et al., 2013) or a combination of these factors (Greene et al., 2009). We hypothesis that nanoplastics might represent a novel environmental factor for neural tube defects, based on the work that we (Wang et al., 2023) and others (Nie et al., 2021; Yan et al., 2020) have published showing nanoparticle-induced neural tube defects in the chick

embryo. As neural tube defects are caused by a failure of neurulation, I shall now discuss the various mechanisms involved in neural tube development (neurulation).

There are two types of neurulation during the development of chick embryo, namely, primary neurulation and secondary neurulation (Schoenwolf, 2018; Shimokita and Takahashi, 2011; van der Spuy et al., 2023). Primary neurulation is the rolling-up of the neural plate to form a hollow tube, whereas secondary neurulation is the formation of a solid neural keel which secondarily becomes hollow (Dady et al., 2014). We have observed neural tube defects related to both of these processes (Chapter 2). Therefore, it is likely that PS-NPs disrupt the primary and/or neurulation of developing chick embryos. It is still unclear the mechanism underlying the NTDs caused by PS-NPs exposure.

In addition to neural tube defects observed in PS-NPs treated chick embryos (Chapter 2), we also noticed, on histological sections, an anomalous clump of cells located in lumen of neural tube. We speculated that these were likely neural crest cells, based on their location. This hypothesis is strengthened by the fact that these cells express the neural crest marker TFAP2A (Chapter 3). Neural crest cells are an embryonic population of migratory stem cells (Achilleos and Trainor, 2012). In birds, neural crest cells arise from the margins of the neural ectoderm and become localized to the neural folds (Le Douarin, 2004). After the neural folds meet in the dorsal middle line, the neural crest cells start to detach from the ectoderm and migrate through the mesoderm into various tissue and organs (Le Douarin, 1999). These migratory cells differentiate into various cell types, contributing to the development and function of multiple organs (Kirby and Waldo, 1995; Martik and Bronner, 2021; Waldo et al., 1999).

In this research, we want to investigate the possible mechanism of how PS-NPs cause neural tube defects. We want to use *in situ* hybridization to identify the potential tissue or cell population which has been affect by PS-NPs. *In situ* hybridization is a tool for locating mRNA transcripts in whole specimens (‘wholemount *in situ*

hybridization') or sections (Wilkinson, 1998). this technique is widely used in biomedical research (Chu et al., 2019). We have selected several highly conserved genes as markers (Table 2) for the neural crest, according to the literature (Martik and Bronner, 2021), and then examined them using wholemount *in situ* hybridization. The aim of this chapter is to investigate the how polystyrene nanoparticles affect neurulation, and possibly the neural crest, casing malformations.

Materials and Methods

Sample collection and preparation

We used the same materials and techniques as described in detail in Chapter 2. Briefly, surviving embryos exposed to 25 nm plain nanoplastics were fixed in 2% PFA in PBS at 4 °C overnight. Fixed embryos were then rinsed in PBS and dehydrated through methanol series (25%, 50%, 70% and 100%) and stored at -20 °C in 100% methanol. All embryos were staged according to Hamburger and Hamilton (Hamburger and Hamilton, 1951).

RNA extraction and cDNA synthesis

The RNA was isolated from stage 13-16 chick embryos by TRIzol™ Reagent (Thermo Fisher Scientific, USA) in house followed by purification with RNeasy Mini Kit (50; Qiagen, Venlo, Netherlands). The concentration of purified RNA was measured by Nanodrop. To generate first strand cDNA, we performed two-step reverse transcription polymerase chain reaction (RT-PCR) using SuperScript III (Invitrogen™, USA). The cDNA was diluted 10 ×with DNA- and RNA-free water and stored at -20 °C (Sigma).

Probe synthesis

This protocol is as previously described by us (de Bakker et al., 2013). In brief, we isolated total RNA from an embryo using TRIzol (Invitrogen) and carried out reverse transcription using SuperScript III (Invitrogen). PCR was performed on these

templates using specific primers (Table 4-1; Table S4), and the PCR products were cloned in the TOPOTA-PCRII vector (Invitrogen™). The inserted amplicons were checked by a PCR with M13-pUC primers located on the TOPOTA-PCRII plasmid and checked on an agarose gel. When they were of the right size they were sent for Sanger sequencing (BaseClear B.V., Leiden). After checking the sequence by BLAST searching, the positive results were used as templates for making the digoxigenin labelled antisense RNA probes. See Table S4 for accession numbers.

Table 4-1. **Details of gene markers used for in situ hybridization.**

Gene	Expressed	Location expressed	Reference
FOXD3 (Forkhead box D3)	(pre-)migratory neural crest	Dorsal neural tube, neural folds and head mesenchyme	(Dottori et al., 2001; Fairchild et al., 2014)
SNAI2 (Snail family transcriptional repressor 2)	(pre-)migratory neural crest	Dorsal neural tube and paraxial mesoderm	(Jhingory et al., 2010)
WNT1(Wnt family member 1)	neural crest	Dorsal neural tube Rhombencephalon and mesencephalon	(Brown and Zervas, 2017; Galli et al., 2014)
SOX10 (SRY-box 10)	neural crest	Neural crest and central nervous system	(Cheng et al., 2000)
LMO4 (LIM domain only 4)	neural crest	Neural plate and neural crest	(Ferronha et al., 2013)
PAX3 (Paired box 3)	neural crest	Neural crest and somite	(Bothe and Dietrich, 2006; Goulding et al., 1994)
TFAP2A (Transcription factor AP-2 alpha)	neural crest	Neural plate and Neural crest, pharyngeal arches, ectoderm, cleft	(Poelmann et al., 2017; Wang et al., 2011)

Whole mount *in situ* hybridization

In this study, all gene names are according to Ensembl for *Homo sapiens* (https://www.ensembl.org/). This wholemount protocol is as previously described by us (de Bakker et al., 2021). In brief, embryos were fixed in 2% buffered depolymerized pPFA for 24 h at 4 °C. They were then washed 3 × with cold PBS and dehydrated through a graded methanol series (25%, 50%, 75% and 100%) and stored at -20 °C . Embryos were rehydrated through a graded methanol series, lightly digested with proteinase K (10 mg/mL in PBS) for 5 min and postfixed in 4% buffered pFA in PBS after several washes in PBST (PBS pH 7.2 with 0.1% Tween-20). This was followed by a prehybridization step at 60 °C for at least 3 h or until the embryo had sunk. The hybridization mixture consisted of: 50% formamide, 2% Boehringer blocking powder, 5 × SSC (from 20× standard sodium citrate buffer, 3M sodium chloride, 0.3M sodium citrate, pH 7), 1mg/mL total RNA, 50 µg/mL heparin, 0.1% Triton X-100, 0.1% CHAPS (3-[(3-cholamidopropyl) dimethylammonio]-1-propanesulfonate) and 5mM ethylenediaminetetraacetic acid (EDTA). After the prehybridization mix was removed, we added 400 ng/mL specific probe to fresh hybridization mixture preheated to 60 °C. The embryos were incubated in this mix at 60 °C overnight with slow shaking. The next day, the specific probe mixture was removed, collected and stored at -20 °C for re-use. Several stringent washes were done at 60 °C to remove non-specifically bound probe [2× SSC, 0.1% CHAPS, 50% formamide]; [2× SSC 0.1% CHAPS]; [0.2× SSC, 0.1% CHAPS]. After washing several times at room temperature with TBST (0.1M tris [tris (hydroxymethyl)aminomethane] buffered saline, pH 7.5, 0.1% Tween-20) the embryos were preincubated with heat-inactivated 10% sheep serum in TBST for 90 min at room temperature followed by overnight incubation with sheep anti-digoxigenin conjugated to alkaline phosphatase (Roche; 1:5,000 dilution in 10% sheep serum in TBST at 4 °C overnight).

The next day, the non-specifically bound antibodies were washed away by several washes with TBST of which the last one was overnight at 4 °C. The embryos were brought to a higher pH by washing 3x 10 min in NTT buffer (0.1M sodium chloride,

0.1M Tris/HCl, 0.1% Tween-20, pH 9.5). The enzyme reaction of alkaline phosphate with BM purple (Roche) as substrate results in a blue precipitate. The development of the stain was checked regularly and stopped by washing several times in TBST, removing the substrate and chromogens, and lowering the pH.

Wholemount TUNEL staining

This protocol has been described by us (de Bakker et al., 2021). In brief, embryos were collected and fixed as for *in situ* hybridization, rehydrated through a graded methanol series, and washed in TBST (0.1M tris-buffered saline containing 0.1% Tween). Next, they were pre-treated with proteinase K (10 mg/ml, 5 min at room temperature), washed in TBST, postfixed with 4% formaldehyde in PBST, washed in TBST followed by a wash in the TdT buffer (30 mMTris/HCl, 140 mM Na-cacodylate, 0.1% Triton pH 7.2). They were then preincubated in the reaction mix (70 nM digoxigenin-labeled dUTP, 400 nM ATP, and 1 U/mL terminal transferase in the enzyme buffer) at 4 °C without the cofactor CoCl2 which was added to the reaction mix (1mM end-concentration) after 1 h. With CoCl2 added, the embryos were incubated at room temperature overnight. The reaction was stopped by adding 200 mM EDTA (ethylenediaminetetraacetic acid), pH 7.0, ⅒ of the reaction volume. The digoxygenin-labelled nucleotides were localized with a standard anti-digoxigenin antibody conjugated to alkaline phosphatase procedure followed by staining with BM-purple.

TUNEL staining on paraffin sections

The following protocol has been described by us previously (de Bakker et al., 2021). The protocol was slightly modified by us. Briefly, chicken embryos were fixed and dehydrated as above were, rinsed in 100% ethanol followed by xylene, embedded in paraffin wax, sectioned at 7 µm and mounted on silane-coated slides (VWR International B.V, Amsterdam). The dewaxed slides were treated with 10 µg/mL proteinase K in PBS for 5 min, postfixed in 4% formaldehyde in PBS. The TUNEL reaction took place at 37 °C for 2 h in a similar reaction mix as above but with a

higher concentrations of digoxygenin-labeled dUTP (3.5 µM) and ATP (20 µM) and CoCl2 already added to the mix. The reaction was stopped by rinsing the slides in 20 mM EDTA in PBS. TUNEL-positive cells were localized with a standard anti-digoxigenin antibody conjugated to alkaline phosphatase followed by staining with BM-purple. As a counter stain we used 0.1% neutral red.

Vibratome sectioning

Embryos processed for wholemount *in situ* hybridization and TUNEL were stored in 1% pFA in PBS. They were soaked in a mixture of 30% BSA, 20% sucrose and 0.5% gelatin in PBS as the embedding mixture. The albumin/gelatin was made by dissolving 0.49 g of gelatin (Sigma Cat. No. G1890) in warm PBS (100 mL). The mixture was then cooled to room temperature and 30 g of bovine albumin (Sigma Cat. No. A-4503) added and allowed to dissolve (for several hours). Finally, 20 g sucrose was added. The embryos were then placed in 3 mL of fresh albumin/gelatin mixture in plastic embedding moulds and 240 µL of 10% glutaraldehyde was added as a hardener. The solidified cubes were trimmed and sectioned at 70 µm in Milli-Q® water and mounted on glass slides with 99.5% glycerol.

Localisation of fluorescent 25 nm PS-NPs *in ovo* and *in vitro*

Stage 8 Hamburger-Hamilton chicken embryos were exposed to PS-NPs as described in Chapter 2 under '*In ovo* embryo toxicity experiments' with the exception that, instead of plain PS-NPs, we used green fluorescent polystyrene nanoparticles (cat. number FGP25; 1% solid, 1.05 g/cm^3). The embryos were returned to the incubator and re-incubated for 2, 6 and 24 h. They were then removed from the egg and visualized as wholemounts by confocal microscopy (Zeiss Airyscan 900).

Chicken embryo neural crest cultures

For neural crest cultures, Hamburger-Hamilton 58 stage 14-15 embryos were removed from the egg, and rinsed with sterile calcium-magnesium free Dulbecco's PBS (CMF; Corning®, New York). The method of Cohen and Konigsberg was used

(Cohen and Konigsberg, 1975), slightly modified. In brief, a segment of the embryo body from the axial levels of the last 6-9 somites was cut out using tungsten needles and placed in 0.25% Trypsin-EDTA (Sigma-Aldrich, Zwijndrecht, Cat. No. T4049) on ice for 8-10 min, when the somites and neural tube appeared to be beginning to separate from the surrounding tissues. The segments were then transferred to DMEM (Sigma-Aldrich, Zwijndrecht, D0819) 15% foetal calf serum (Sigma-Aldrich, Zwijndrecht, Cat. No. F7524) and 1% antibiotic-antimycotic (Sigma-Aldrich, Zwijndrecht, Cat. No. A5955).

The tissue pieces were gently triturated with a blue Gilson pipette tip (with the tip cut off and the cut surface polished in a flame). Then, neural tubes and somites were plated into separate µ-Dish 35 mm high glass-bottom dishes (ibidi GmbH; Gräfelfing, Germany,) which we pre-coated with rat-tail collagen type-I (ibid Cat. No. 50201), according to the manufacturer's instructions. The µ-Dishes contained 1 mL culture medium (MEM, HEPES, GlutaMAX™ Supplement (42360, Gibco™ with 15% foetal calf serum and 1% antibiotic-antimycotic). Most of the medium was then aspirated leaving the tissue samples pressed against the substratum by surface tension. They were incubated for 4 h (in 5% CO_2, 37 ° C) until attached and then 1 ml culture medium was added. They were returned to the CO2 incubator and cultured overnight.

We exposed these 2 d cultures of chick neural crest to fluorescent PS-NPs (25 nm). This was done by aspirating the culture medium and replacing with 1 mL fresh culture medium containing PS-NPs at a final concentration 0.1 mg/mL. After incubating for 2 or 6 h at 37 ° C, in 5% CO_2, the culture medium containing PS-NPs was aspirated and the cultures rinsed 3 x with warm culture medium then stained with 5 µg/mL DAPI (4',6-diamidino-2-phenylindole; Invitrogen™) in culture medium for 20 min at 37 ° C. The cultures were rinsed with plain, fresh medium and observed as living cultures under a Zeiss Airyscan 900 confocal microscope fitted with warmed air chamber (37 °

C) to maintain the cultures. The warmed air chamber was an XL-LSM S1 123, connected to Heating Unit XL S and TempModule S (all from Zeiss).

Cryosections

Embryos were fixed with 4% pFA in PBS and then transferred to 30% sucrose solution in PBS (4 h, 4 °C). They were then transferred to OCT embedding matrix (Carl Roth, Karlsruhe) 1 h (4 °C) then transferred to fresh OCT in a plastic mould and snap-frozen in liquid nitrogen. Sections were cut at 25 µm using a Leica CM3050S cryostat and mounted on glass microscope slides. The slides were analyzed using Zeiss Axioplan 2 aka DIC.

Transmission electron microscopy

Primary trunk neural crest cultures were prepared as described above under 'Localisation of fluorescent 25 nm PS-NPs *in ovo* and *in vitro*'. They were cultured on Thermanox coverslips (24 mm ⌀; Thermo Fisher Scientific™) pre-coated with rat-tail collagen type-I, placed into µ-Dish 35 mm high glass-bottom dishes (ibidi GmbH; Gräfelfing, Germany,). The cultures were exposed to 0.1 mg/mL plain PS-NPs 25 nm (1 mL) for 1 h. Coverslips were carefully transferred to 6-well plates and fixed with 2% glutaraldehyde and 2% formaldehyde in sodium cacodylate buffer (0.1 M, pH 7.2) for 2 h. Samples were then incubated with 1% osmium tetroxide with 0.8% potassium ferrocyanide in water for 1 h. After rinsing, they were stained *en bloc* with 1% uranyl acetate in water. The staining of the samples was checked under a Zeiss Observe Z1 inverted fluorescence microscope before further process (Fig. S1). The samples were dehydrated through a graded ethanol series (70%, 90%, 100%, 1 h each). Finally, they were embedded in Agar 100 resin kit (cat. number R1031, Agar Scientific, Essex, UK) using propylene oxide as the intermediate reagent, and sectioned at 70 nm using a diamond knife. The sections were examined using a JEOL 1400+ electron microscope.

Results

Nanoplastics become localized to the dorsal middle of the neural tube

To track the distribution of PS-NPs, stage 8 chicken embryos were exposed *in ovo* to 50 µL (0.1 mg/mL) fluorescein-labelled 25 nm PS-NPs for 2, 6 and 24 h. Confocal imaging showed that that fluorescence became localized in cell masses in the dorsal midline of the neural tube (Fig. 4-1a-c). This corresponds to the region where neural crest cells develop. Labelled cell masses were also seen protruding into the lumen from the dorsal aspect of the neural tube, or lying free in the lumen (Fig. 4-1d).

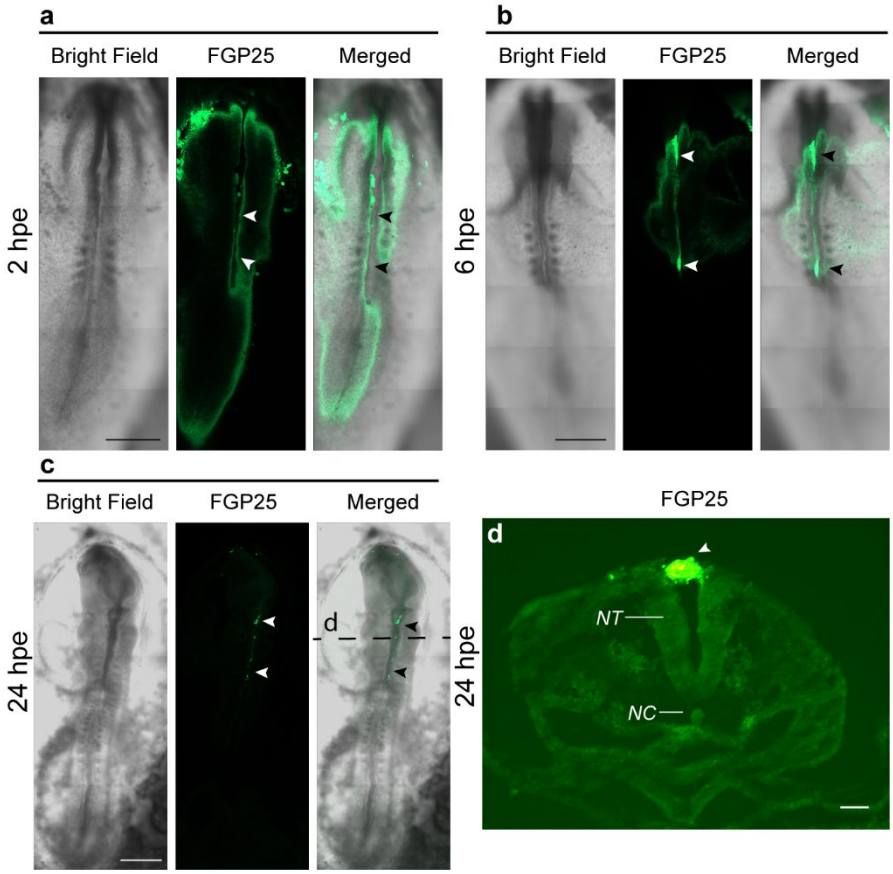

Fig. 4-1. **25 nm green fluorescent polystyrene nanoparticles adhere to the dorsal middle line and lying between the neural folds. a**-**c**, chick embryos exposed to fluorescent PS-NPs (FGP, green florescence) examined at 2, 6 and 24 h, respectively. *n* = 2 for all different time series. **a**, 2 hpe PS-NPs treated chick embryos, stage 8. **b**, 6 hpe PS-NPs treated chick embryos, stage 9. **c**, 24 hpe PS-NPs treated chick embryos, stage 13. In **a**-**c**, there is strong fluorescence *(Copp et al.)* associated with the dorsal midline of the neural tube (black and white arrowheads; note that the chicken embryos did not show autofluorescence). **d**, transverse cryosection (25 µm). There is strong fluorescence *(Copp et*

al.) in a cellular mass lying in between the neural folds (white arrowheads). Key, hpe, hours post-exposure. Note, NC, notochord, NT, neural tube. Scale bars, 500 µm in **a**-**c** and 50 µm in **d**.

Nanoplastics disrupt the development of neural crest cells

To confirm the neural crest identity of the affected cells, we studied the expression of a panel of neural crest markers, namely: WNT1, FOXD3, SNAI2 (SLUG, SNAIL2), LMO4, SOX10, PAX3 and TFAP2A (Table 4-1 and Table S4). In PS-NP treated embryos, we found that the cells remaining in the dorsal midline, or the margins of the open neural tube, express neural crest markers (Fig. 4-2, Fig. 4-3, and Fig. 4-4). These findings were consistent across all seven neural crest markers (Fig. 4-2, Fig. 4-3, and

Fig. 4-4).

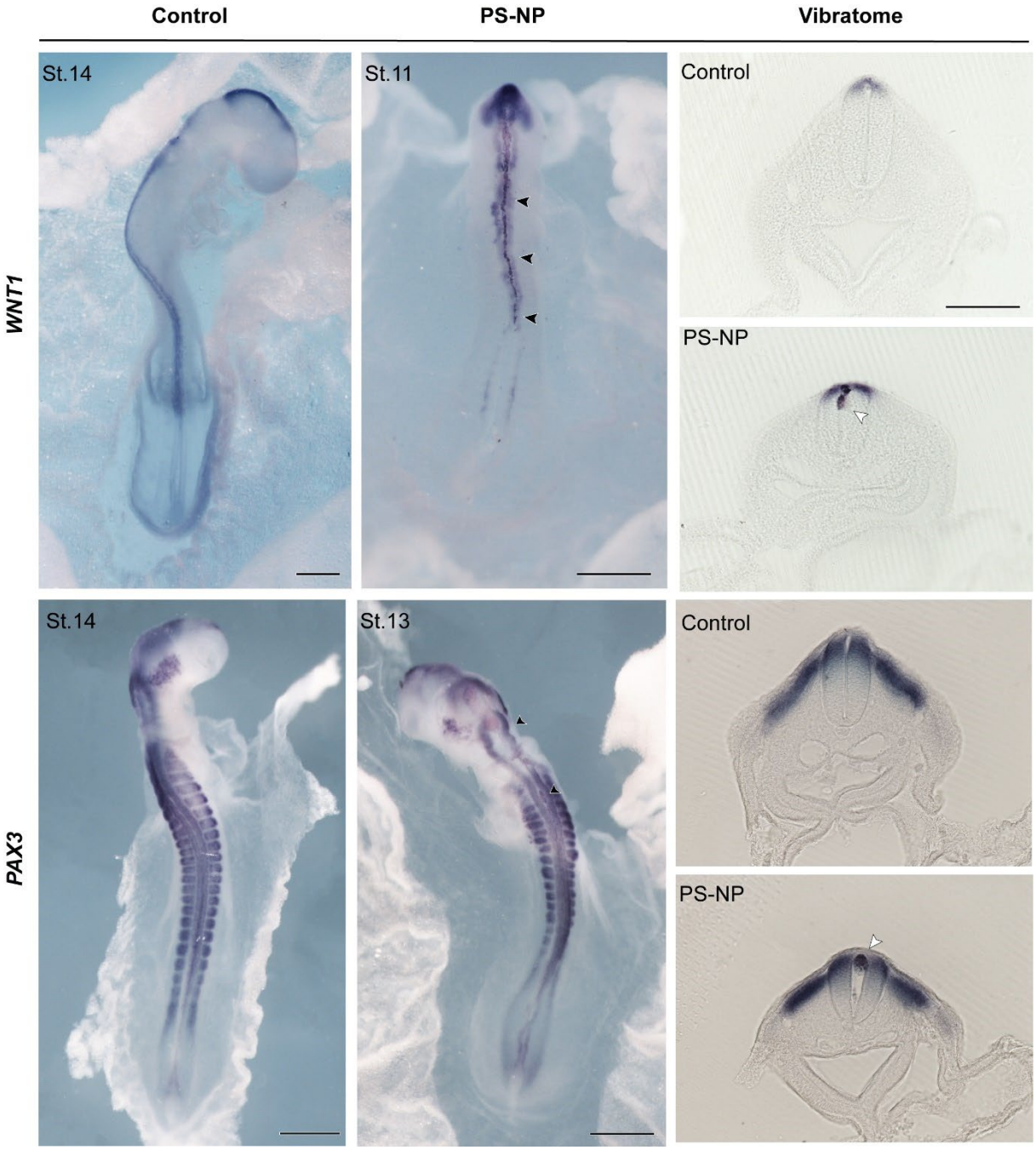

Fig. 4-2. **Cells disrupted by 25 nm PS-NPs express neural crest markers (*WNT1* and *PAX3*)**. Embryos were exposed at stage 8 to 50 µL plain PS-NPs (5 mg/mL) or Ringer's only. *n* = 3 for both control and PS-NP treated group of all genes. *Note*, all embryos are two days incubation; the treated embryos all showed developmental delay relative to the controls. Cellular debris of neural crest cells (black arrowheads). *Note*, White arrowheads in the treated embryos indicate putative neural crest cells. *Key*: hpe: hours post-exposure, PS-NP, embryos treated with polystyrene nanoparticles, 25 nm, 5 mg/mL. Scale bars, 500 µm in wholemount embryos, and 200 µm in vibratome transverse sections.

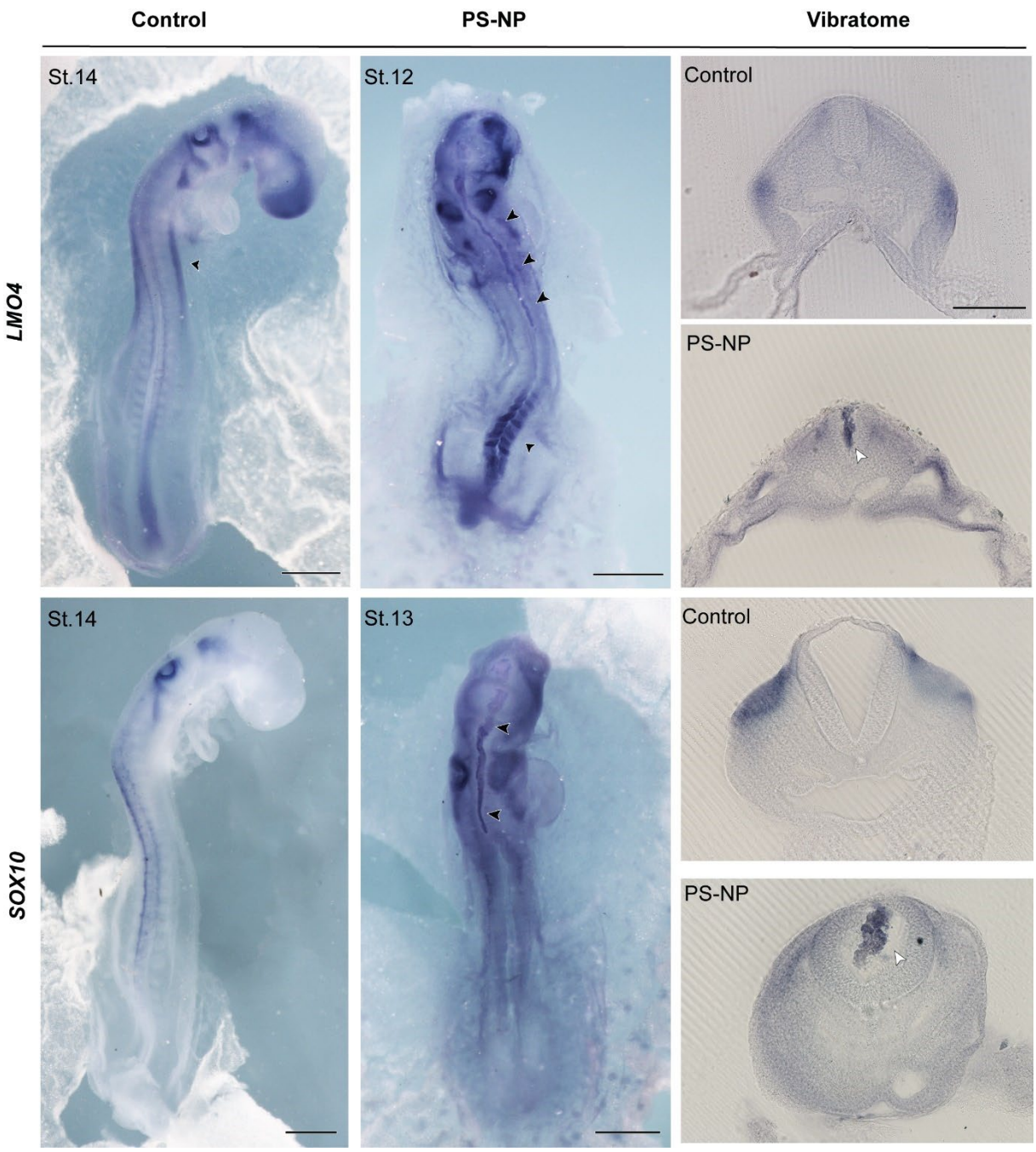

Fig. 4-3. **Cells disrupted by 25 nm PS-NPs express neural crest markers (*LMO4* and *SOX10*).** Embryos were exposed at stage 8 to 50 µL plain PS-NPs (5 mg/mL) or Ringer's only. *n* = 3 for both control and PS-NP treated group of all genes. *Note*, all embryos are two days incubation; the treated embryos all showed developmental delay relative to the controls. Cellular debris of neural crest cells (arrowheads). *Note*, White arrowheads in the treated embryos indicate putative neural crest cells. *Key*: hpe: hours post-exposure, PS-NP, embryos treated with polystyrene nanoparticles, 25 nm, 5 mg/mL. Scale bars, 500 µm in wholemount embryos, and 200 µm in vibratome transverse sections.

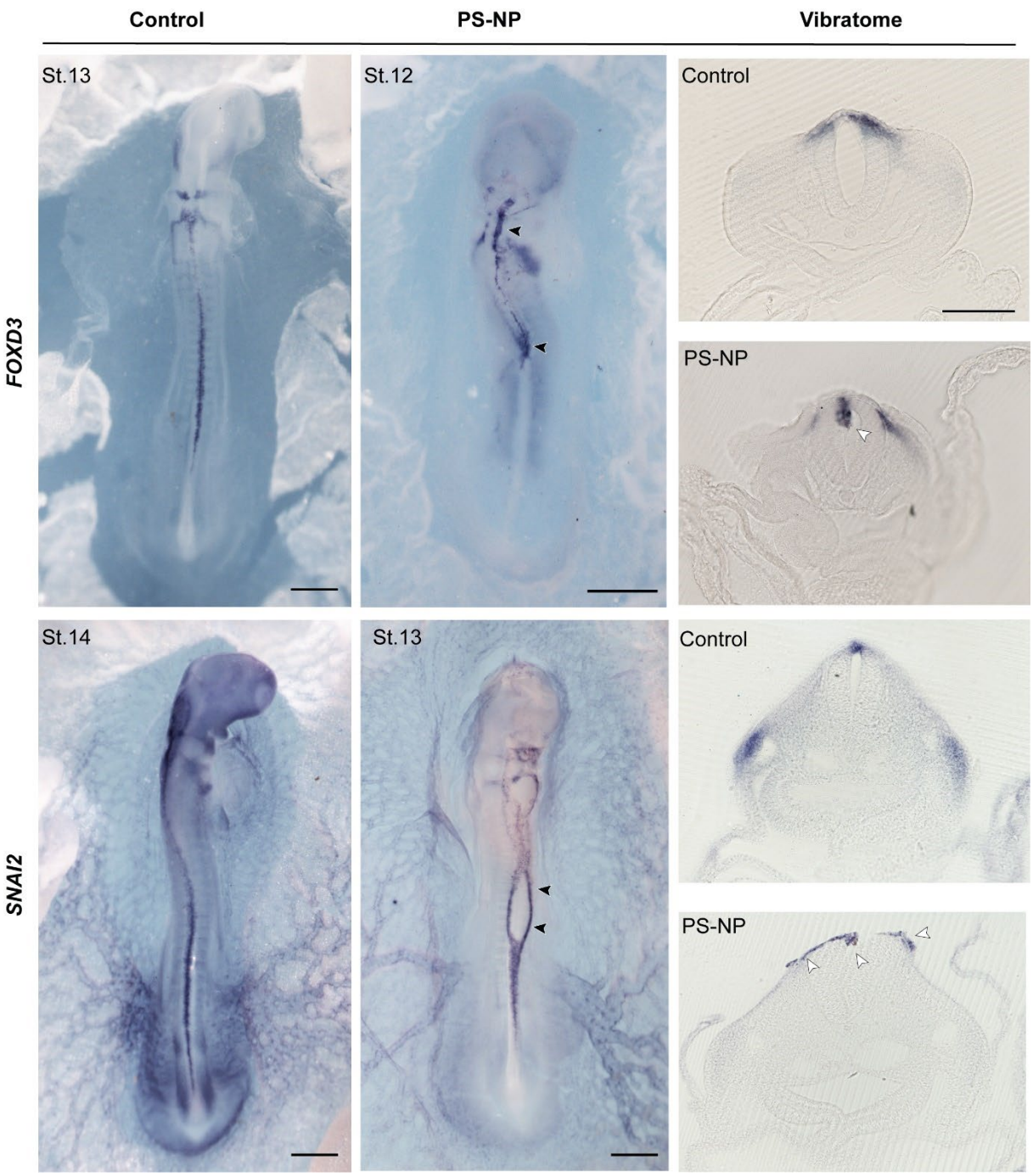

Fig. 4-4. **Cells disrupted by 25 nm PS-NPs express neural crest markers (*FOXD3* and *SNAI2*)**. Embryos were exposed at stage 8 to 50 µL plain PS-NPs (5 mg/mL) or Ringer's only. *n* = 3 for both control and PS-NP treated group of all genes. *Note*, all embryos are two days incubation; the treated embryos all showed developmental delay relative to the controls. Cellular debris of neural crest cells (black arrowheads). *Note,* White arrowheads in the treated embryos indicate putative neural crest cells. *Note*, In the FOXD3 *in situs*, the cells are clumped. In the SNAI2 *in situs*, there are putative neural crest cells that are margins of the neural tube defects. Scale bars, 500 µm in wholemount embryos, and 200 µm in vibratome transverse sections.

Nanoplastics can enter neural crest cells

To understand the interaction between PS-NPs and neural crest cells, we have exposed primary cultures of chicken embryo neural crest cells to PS-NPs (Fig. 4-5). We found that the cells showed an uptake of fluorescent PS-NPs within 2–6 h (Fig. 4-5d-f) as indicated by the appearance of fluorescence in the cytoplasm. Transmission electron microscopy of the cultured cells showed inclusions or lacunae that were consistent with PS-NPs in the cytoplasm (Fig. 4-6).

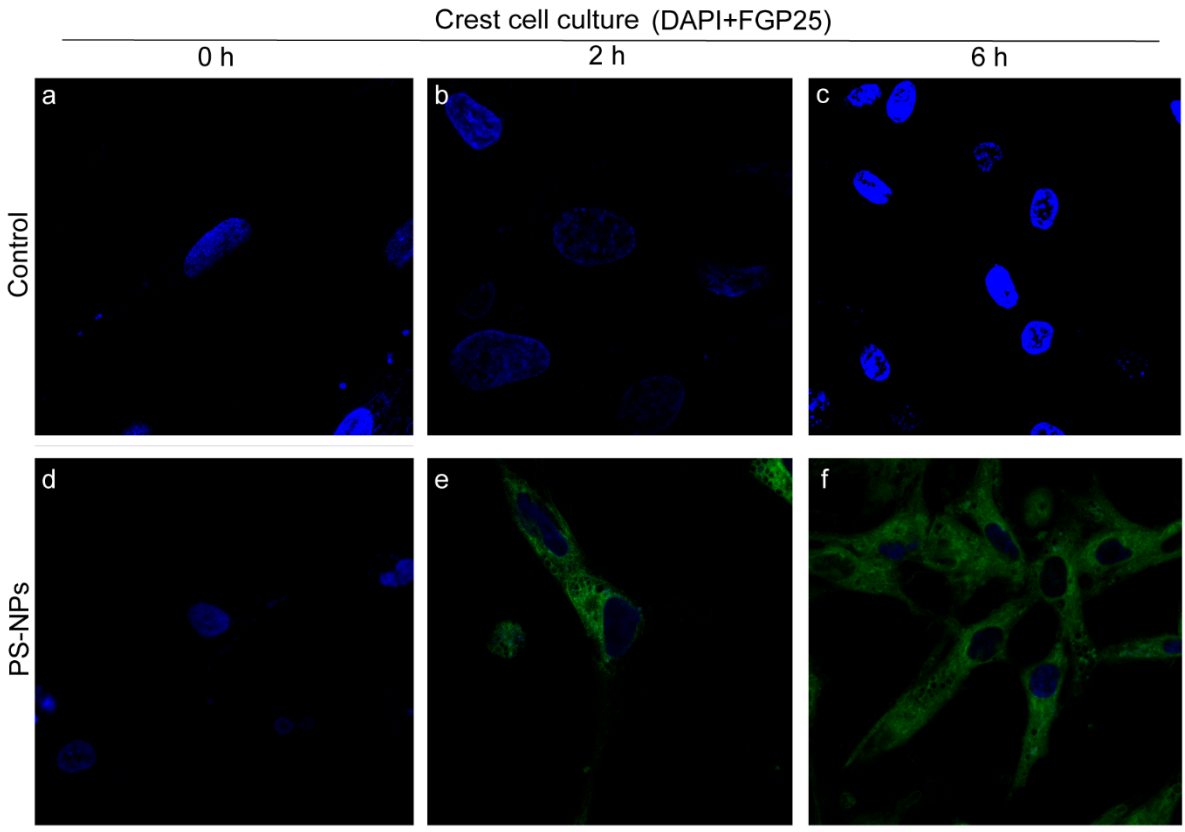

Fig. 4-5. **Fluorescent polystyrene nanoplastics (25 nm) become co-localized to primary neural crest cells *in vitro***. **a**-**c**, neural crest cells stain with DAPI (blue florescence) exposed in vitro to Ringer's solution and examined at 0, 2, and 6 h, respectively. **d**-**f**, neural crest cells stain with DAPI (blue florescence) exposed in vitro to fluorescent PS-NPs (green florescence) and examined at 0, 2, and 6 h, respectively.

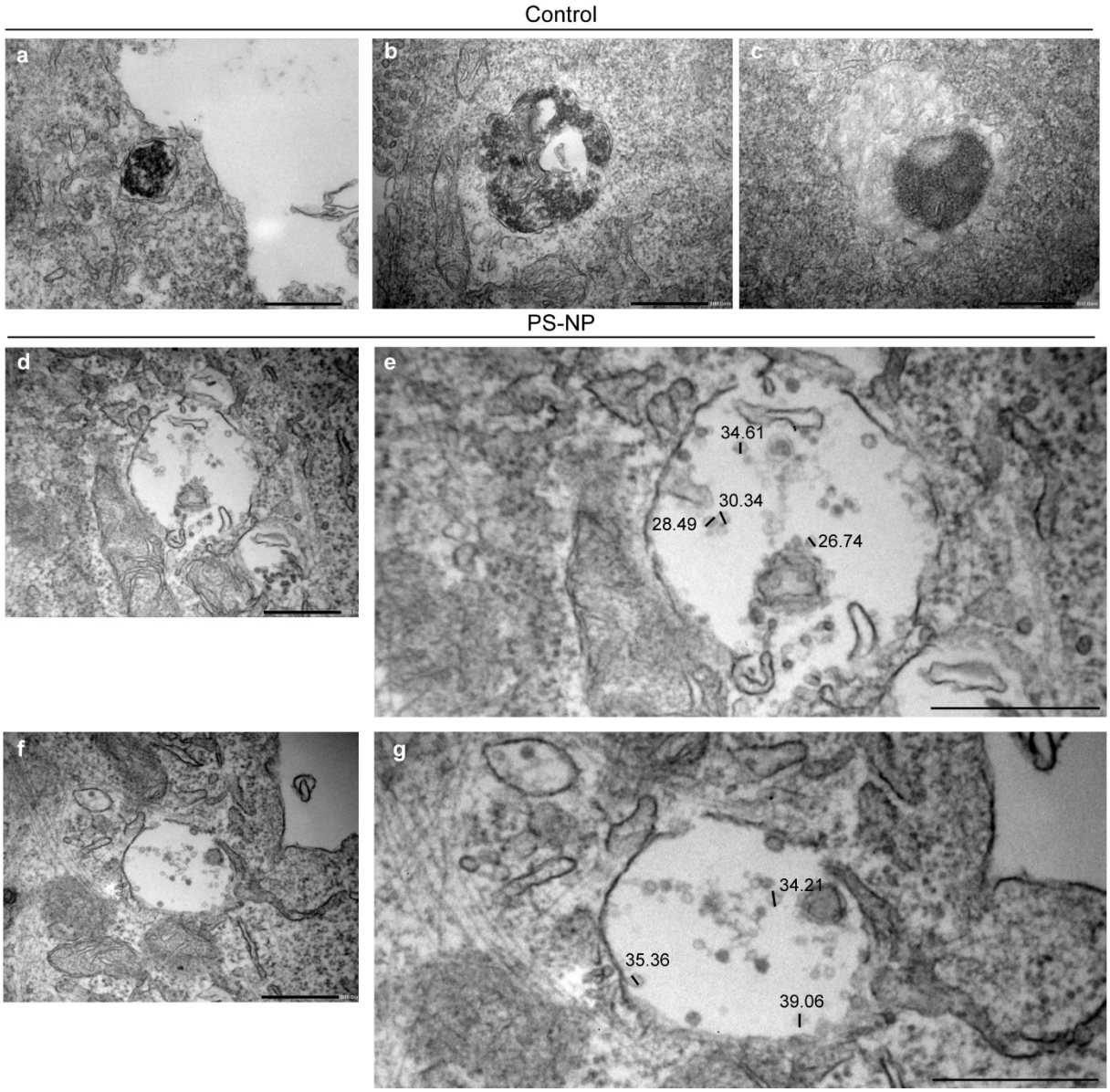

Fig. 4-6. **Transmission electron microscopy of 2 d chicken embryo neural crest cultures 1 h after exposure to PS-NPs (0.1 mg/mL) in culture medium**. **a**-**c**, controls (culture medium only); **d**-**g**, PS-NP-treated. In the treated cultures, spheres of 26.74—39.06 nm were observed. These near-perfect spheres lacked any sign of a membrane (biological membranes will appear dark because of the osmium tetroxide treatment). According to several reports in the literature (Domenech et al., 2021; Qiao et al., 2021), such spherical structures may represent nanoplastic particles. In any case, we present these findings as only tentative identification of PS-NPs. To make a positive identification of PS-NPs with TEM would require — for example — the use of PS-NPs with a gold core. *Note,* also that our confocal imaging studies do support the idea of uptake of PS-NPs by neural crest cells in Fig. 4-3). *Key*: scale bars, 500 nm.

Nanoplastics cause cell death in presumptive neural crest cells

We performed TUNEL assay on wholemount control and PS-NPs-treated embryo at 24 hpe. When we examined the dorsal aspect of the wholemount embryos, we saw

only a few, scattered cells positive for TUNEL label in control (Fig. 4-7a). Vibratome sections showed that these cells were located in the dorsal ectoderm and neural folds (Fig. 4-7d). In the PS-NP treated embryos, the numbers of TUNEL-positive cells were greatly increased (Fig. 4-7b and c). These labeled cells, like those in the control embryos, were visible in the dorsal ectoderm in vibratome sections, and surrounding the neural folds (Fig. 4-7e-g). In addition, clumps of TUNEL-positive cells were seen in the lumen of the neural tube (Fig. 4-7e-g). We observed similar results with TUNEL staining on paraffin sections, which showed clumps of putative dead cells in the lumen of the neural tube (Fig. 4-7h-k).

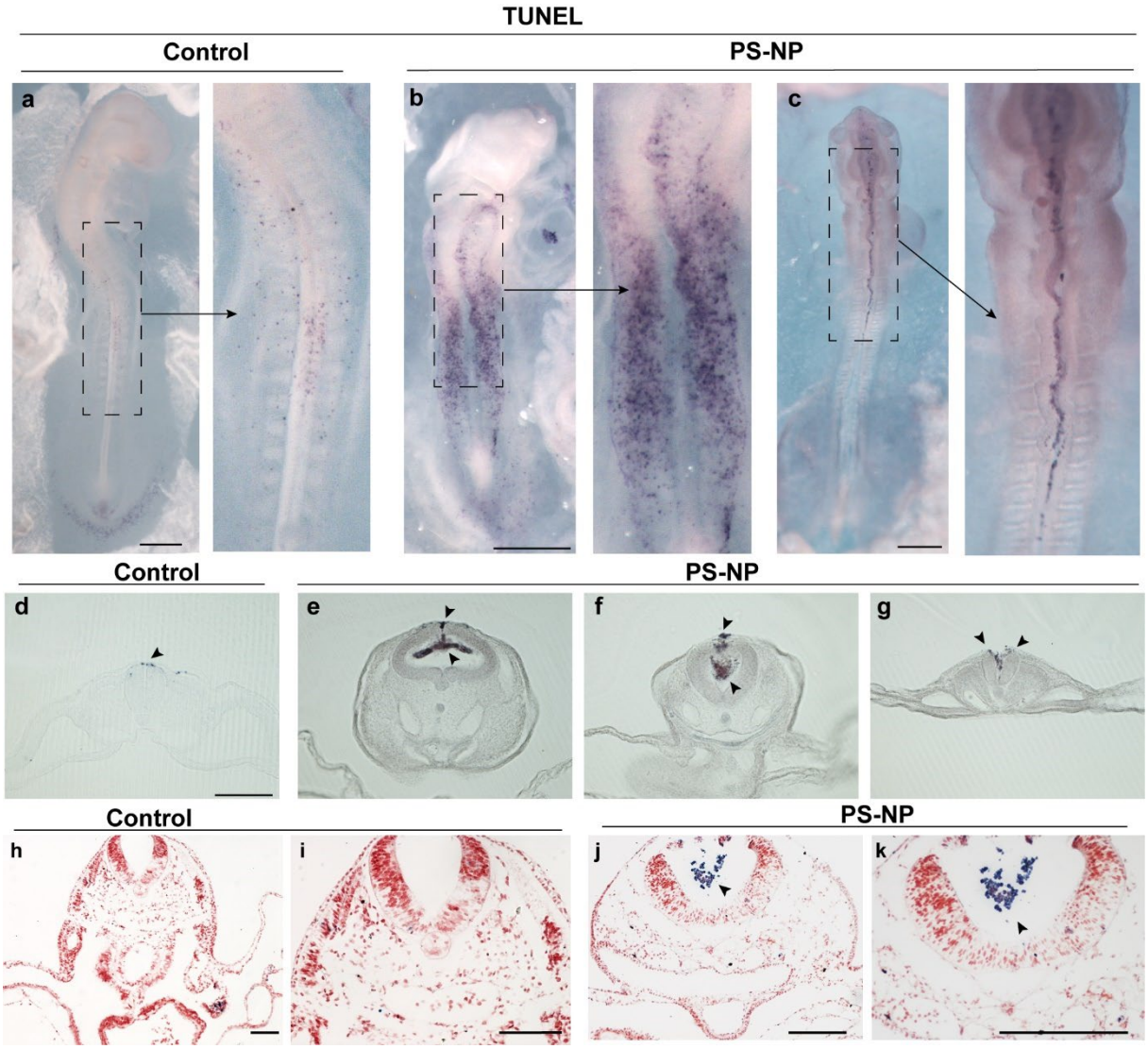

Fig. 4-7. **Exposure of stage 8 chicken embryos to plain polystyrene nanoparticles induces cell death in putative neural crest cells**. Figures show embryos 24 hpe. Wholemount TUNEL staining of control (**a**) and PS-NP-treated (**b** and **c**) chick embryos. *n* = 2 for control and *n* = 3 for PS-NP treated group. (**a**), stage 14, (**b**), stage 12, (**c**), stage 12 (Note all embryos are 2 d incubation, but **b** and **c** show a

developmental delay caused by PS-NP treatment. In **b** and **c**, note the extensive cell death, and dead cells in the dorsal midline. **d**-**g**, TUNEL staining on vibratome sections. *n* = 2 for both control and PS-NPs-treated chick embryos. **d**, control, stage 14. **f**-**g**, PS-NPs-treated, stage 12. PS-NPs treatment resulted in clumps of dead cells in the neural folds and in the neural tube lumen (black arrowhead). **h**-**k**, TUNEL staining on paraffin sections of control embryo (**h** and **i**), and PS-NPs treated embryo (Smits-van Prooije et al.), *n* = 2 for both groups. *Note*, massive cell death lying free in the lumen of neural tube (**j** and **k**). *Key*, 500 µm in **a**-**c**, 200 µm in **d**-**k**.

Discussion

It has been reported that 60 and 900 nm NPs can have harmful effects on the developing chick embryo (Nie et al., 2021). Those negative effects include neural tube defects and development delay (Nie et al., 2021). In our previous research (Chapters 2 and 3), we found a much wider spectrum defects, including defects in cardiovascular and craniofacial tissues, eyes, tail-bud, and vertebral column defects in the PS-NPs treated embryos. The previous study suggested that PS-NPs were taken up through caveolae-mediated endocytosis into nerve cells (Nie et al., 2021). After entering the cells, PS-NPs induce autophagy and apoptosis leading to neural tube defects (Nie et al., 2021). However, these suggested mechanisms could not easily account for the major malformations that we have described in Chapters 2 and 3. We agree that PS-NPs can damage cells in the location of the neural tube since we also observe dead cells surrounding the neural folds (this chapter). However, compared to the dead cells we saw in the lumen, very few cells in the neural tube itself were stained by the TUNEL protocol. Therefore, we explored mechanisms alternative to a simple effect of PS-NPs on the neural tube itself.

To explore this possibility, we first conducting experiments in which we tracked distribution of fluorescent PS-NPs in the chick embryo. We saw that many PS-NPs become localized to the dorsal middle line of the embryo, often attached to clumps of cells in the lumen of the neural tube. We noticed these abnormal clumps of cells in our previous experiments (Chapters 2 and 4). Normally, the lumen of the neural tube does not contain such clumps of cells. We speculate that these cell clusters might be neural crest cells because of their location. This would explain why we and the

previous authors observed neural tube defects: the normal migration of neural crest cells is thought to be essential to the neural tube closure (Copp et al., 2003; Ewart et al., 1997; Morris-Kay and Tan, 1987). Therefore, the neural tube defects we observed in our research may caused by the disruption of PS-NPs to the migration of neural crest cells.

To further examine the possible neural crest identity of the cells disrupted by PS-NPs, we examined the expression of six neural crest markers in PS-NPs-treated and control embryos at 24 hpe. Interestingly, we found that the expression of all neural crest markers – except SNAI2) – is consistent with our hypothesis that the abnormal cells in PS-NP treated embryos are putative neural crest cells. Interestingly, in this context, it has been reported that the exposure of developing chick embryos to zinc oxide nanoparticles leads to abnormal migration of cranial neural crest cells (Yan et al., 2020). Therefore it is possible that neural crest are sensitive to nanoparticles more generally.

In addition, the dysplasia we saw in the craniofacial tissue of PS-NPs-treated embryos (Chapter 3), could be explained by the same mechanism: disruption of neural crest cells. Cranial neural crest cells play a crucial role in head morphogenesis. This is because they migrate in prosencephalic and mesencephalic streams into the facial region (Martik and Bronner, 2021; Santagati and Rijli, 2003). Moreover, the exposure of chick embryos to high glucose concentrations, disrupts the migration of cranial neural crest cells, resulting in abnormalities of the facial skeleton (Wang et al., 2015).

In Chapters 2, 3 and 4, we have consistently detected microphthalmia at various stages among PS-NP-treated chick embryos. It has previously been shown that silver and gold nanoparticles can interfere with the development of the eyes in zebrafish (Kim et al., 2013; Lee et al., 2007). Those two studies (Kim et al., 2013; Lee et al., 2007) also suggest that metal nanoparticles disrupt the expression of genes related to eye development, or maybe even influence the development of the central nervous system.

We did not find that fluorescent PS-NPs adhere to, or accumulate in, the eyes of chicken embryos after exposure (this Chapter). Therefore, it is highly unlikely that our observed microphthalmia was caused by PS-NPs directly. Our alternative hypothesis is that the microphthalmia may be caused indirectly by the disruption of neural crest cells. It has previously been shown that neural crest cells are essential for eye development in chick embryos (Grocott et al., 2011). Migrating neural crest cells produce TGF-βs, that activate both SMAD3 and canonical WNT signaling, controlling PAX6 function and transcription (Grocott et al., 2011). Pax6 is a well known gene that play a crucial role in eye development in many species (Chow et al., 1999; Gehring, 1996; Hanson, 2003; Nishina et al., 1999; Onuma et al., 2002).

In Chapter 3, we studied the effects of nanoplastics on the chick embryo cardiovascular system. We also looked at the expression of TFAP2A, a gene expressed in neural crest cells. In this chapter, we have examined six additional neural crest cell markers. The results are consistent across the different stages studied (Chapters 3 and 4) and show that PS-NPs affect the migration of neural crest cells. Furthermore, TUNEL labelling suggests that at least some neural crest cells are damaged, and undergo cell death. Consequently, fewer neural crest cells are able to migrate through pharyngeal arches into heart, resulting in heart ventricle septum and cardiovascular defects (Kirby and Waldo, 1995; Waldo et al., 1999). Moreover, these results are consistent with previous studies of hear development in which the microsurgical ablation of neural crest results in various heart defects, including persistent truncus arteriosus, and ventricular septal defects (Hutson and Kirby, 2007).

Although most of the malformations observed after PS-NP exposure are consistent with neural crest disruption, the tailbud effects and caudal neural tube dysplasia cannot be explained as neural crest defects. In the chick embryo, the tailbud and caudal neural tube are in the caudal region of the embryo where the neural tube is formed by secondary neurulation. Secondary neurulation is the formation of the neural tube as a solid primordium without the folding up of a neural plate (Harrington

et al., 2009). Secondary neurulation therefore takes place process entirely under the surface ectoderm (Catala, 2021). This contrasts with primary neurulation where the neural plate develops two folds (neural folds) which elevate and finally fuse in the midline. During primary neurulation, neural crest cells develop at the margins of the neural plate, where the neural folds develop. The neural crest cells then undergo epithelial-to-mesenchymal transformation (EMT) (Rocha et al., 2020; Schoenwolf and Smith, 1990; Schoenwolf and Smith, 2000).

Because secondary neurulation takes place under (ventral to) the surface ectoderm, and the PS-NPs were dripped onto the dorsal side of the ectoderm, we have to explain how the PS-NPs come in contact with the neural tube forming by secondary neurulation, considering that the caudal neural tube is grossly dysplastic in several treated embryos (Figure 7 in **Chapter 2**). Furthermore, the chick embryo has not start secondary neurulation at stage 8 when we introduce the PS-NPs (Schoenwolf and Smith, 1990). To explain these facts, we suggest an alternative hypothesis whereby PS-NPs may adhere to surface mesenchymal populations in the primitive streak of the tailbud, and thereby entering the region of the developing neural tube via EMT (Bellairs, 1986; Shook and Keller, 2003). Another alternative hypothesis could be that PS-NPs may adhere to cells at the junction between primary and secondary neurulation (Dady et al., 2014). Junctional cells in this region undergo EMT and so it is possible that that PS-NPs may attach to these mesenchymal cells, interrupting their EMT (Dady et al., 2014).

Conclusions

We suggest that the mechanism of the malformations we have observed in our research is that PS-NPs passively target migration neural crest cells disrupting their migration and development. The PS-MPs may also disrupt other cell populations undergoing epithelial-mesenchymal transformation on the dorsal surface of the embryo, specifically the cells of the primitive streak. Finally, PS-NPs cause direct

effect on the caudal neural tube in the junctional area between primary and secondary neurulation. This results in neural tube dysplasia in the cadual region. Future work is needed to identify the molecular interactions that lead PS-NPs to adhere to cells undergoing epithelial-mesenchymal transformation. We also need to know whether these effects are specific to polystyrene plastic nanoparticles or to other types of nanomaterials more generally.

References

Achilleos, A. and Trainor, P. A. (2012). Neural Crest Stem Cells: Discovery, Properties and Potential for Therapy. *Cell Res* **22**, 288-304.

Andrady, A. L., Torikai, A., Redhwi, H. H., Pandey, K. K. and Gies, P. (2015). Consequences of Stratospheric Ozone Depletion and Climate Change on the Use of Materials. *Photochem Photobiol Sci* **14**, 170-184.

Bellairs, R. (1986). The Primitive Streak. *Anatomy and Embryology* **174**, 1-14.

Boehnke, N., Straehla, J. P., Safford, H. C., Kocak, M., Rees, M. G., Ronan, M., Rosenberg, D., Adelmann, C. H., Chivukula, R. R., Nabar, N., et al. (2022). Massively Parallel Pooled Screening Reveals Genomic Determinants of Nanoparticle Delivery. *Science* **377**, eabm5551.

Bothe, I. and Dietrich, S. (2006). The Molecular Setup of the Avian Head Mesoderm and Its Implication for Craniofacial Myogenesis. *Dev Dyn* **235**, 2845-2860.

Brown, S. and Zervas, M. (2017). Temporal Expression of Wnt1 Defines the Competency State and Terminal Identity of Progenitors in the Developing Cochlear Nucleus and Inferior Colliculus. *Front Neuroanat* **11**, 67.

Catala, M. (2021). Overview of Secondary Neurulation. *J Korean Neurosurg Soc* **64**, 346-358.

Cheng, Y.-C., Cheung, M., Abu-Elmagd, M. M., Orme, A. and Scotting, P. J. (2000). Chick Sox10, a Transcription Factor Expressed in Both Early Neural Crest Cells and Central Nervous System. *Developmental Brain Research* **121**, 233-241.

Chow, R. L., Altmann, C. R., Lang, R. A. and Hemmati-Brivanlou, A. (1999). Pax6 Induces Ectopic Eyes in a Vertebrate. *Development* **126**, 4213-4222.

Chu, Y. H., Hardin, H., Zhang, R., Guo, Z. and Lloyd, R. V. (2019). In Situ Hybridization: Introduction to Techniques, Applications and Pitfalls in the Performance and Interpretation of Assays. *Semin Diagn Pathol* **36**, 336-341.

Cohen, A. M. and Konigsberg, I. R. (1975). A Clonal Approach to the Problem of Neural Crest Determination. *Developmental Biology* **46**, 262-280.

Copp, A. J., Greene, N. D. and Murdoch, J. N. (2003). The Genetic Basis of Mammalian Neurulation. *Nat Rev Genet* **4**, 784-793.

Copp, A. J., Stanier, P. and Greene, N. D. (2013). Neural Tube Defects: Recent Advances, Unsolved Questions, and Controversies. *Lancet Neurol* **12**, 799-810.

Dady, A., Havis, E., Escriou, V., Catala, M. and Duband, J. L. (2014). Junctional Neurulation: A Unique Developmental Program Shaping a Discrete Region of the Spinal Cord Highly Susceptible to Neural Tube Defects. *J Neurosci* **34**, 13208-13221.

de Bakker, M. A. G., Fowler, D. A., Oude, K. d., Dondorp, E. M., Navas, M. C. G., Horbanczuk, J. O., Sire, J.-Y., Szczerbińska, D. and Richardson, M. K. (2013). Digit Loss in Archosaur Evolution and the Interplay between Selection and Constraints. *Nature* **500**, 445-448.

de Bakker, M. A. G., van der Vos, W., de Jager, K., Chung, W. Y., Fowler, D. A., Dondorp, E., Spiekman, S. N. F., Chew, K. Y., Xie, B., Jimenez, R., et al. (2021). Selection on Phalanx Development in the Evolution of the Bird Wing. *Mol Biol Evol* **38**, 4222-4237.

Domenech, J., de Britto, M., Velazquez, A., Pastor, S., Hernandez, A., Marcos, R. and Cortes, C. (2021). Long-Term Effects of Polystyrene Nanoplastics in Human Intestinal Caco-2 Cells. *Biomolecules* **11**.

Dottori, M., Gross, M. K., Labosky, P. and Goulding, M. (2001). The Winged-Helix Transcription Factor Foxd3 Suppresses Interneuron Differentiation and Promotes Neural Crest Cell Fate. *Development* **128**, 4127-4138.

Ewart, J. L., Cohen, M. F., Meyer, R. A., Huang, G. Y., Wessels, A., Gourdie, R. G., Chin, A. J., Park, S. M., Lazatin, B. O., Villabon, S., et al. (1997). Heart and Neural Tube Defects in Transgenic Mice Overexpressing the Cx43 Gap Junction Gene. *Development* **124**, 1281-1292.

Fairchild, C. L., Conway, J. P., Schiffmacher, A. T., Taneyhill, L. A. and Gammill, L. S. (2014). Foxd3 Regulates Cranial Neural Crest Emt Via Downregulation of Tetraspanin18 Independent of Its Functions During Neural Crest Formation. *Mech Dev* **132**, 1-12.

Ferronha, T., Rabadán, M. A., Gil-Guiñon, E., Le Dréau, G., de Torres, C. and Martí, E. (2013). Lmo4 Is an Essential Cofactor in the Snail2-Mediated Epithelial-to-Mesenchymal Transition of Neuroblastoma and Neural Crest Cells. *J Neurosci* **33**, 2773-2783.

Galli, L. M., Munji, R. N., Chapman, S. C., Easton, A., Li, L., Onguka, O., Ramahi, J. S., Suriben, R., Szabo, L. A., Teng, C., et al. (2014). Frizzled10 Mediates Wnt1 and Wnt3a Signaling in the Dorsal Spinal Cord of the Developing Chick Embryo. *Dev Dyn* **243**, 833-843.

Gehring, W. J. (1996). The Master Control Gene for Morphogenesis and Evolution of the Eye. *Genes Cells* **1**, 11-15.

Goulding, M., Lumsden, A. and Paquette, A. J. (1994). Regulation of Pax-3 Expression in the Dermomyotome and Its Role in Muscle Development. *Development* **120**, 957-971.

Greene, N. D., Stanier, P. and Copp, A. J. (2009). Genetics of Human Neural Tube Defects. *Hum Mol Genet* **18**, R113-129.

Grocott, T., Johnson, S., Bailey, A. P. and Streit, A. (2011). Neural Crest Cells Organize the Eye Via Tgf-B and Canonical Wnt Signalling. *Nature Communications* **2**, 265.

Hamburger, V. and Hamilton, H. L. (1951). A Series of Normal Stages in the Development of the Chick Embryo. *J Morphol* **88**, 49-92.

Hanson, I. M. (2003). Pax6 and Congenital Eye Malformations. *Pediatr Res* **54**, 791-796.

Harrington, M. J., Hong, E. and Brewster, R. (2009). Comparative Analysis of Neurulation: First Impressions Do Not Count. *Mol Reprod Dev* **76**, 954-965.

Hutson, M. R. and Kirby, M. L. (2007). Model Systems for the Study of Heart Development and Disease: Cardiac Neural Crest and Conotruncal Malformations. *Seminars in Cell & Developmental Biology* **18**, 101-110.

Jhingory, S., Wu, C. Y. and Taneyhill, L. A. (2010). Novel Insight into the Function and Regulation of Alphan-Catenin by Snail2 During Chick Neural Crest Cell Migration. *Dev Biol* **344**, 896-910.

Kim, K. T., Zaikova, T., Hutchison, J. E. and Tanguay, R. L. (2013). Gold Nanoparticles Disrupt Zebrafish Eye Development and Pigmentation. *Toxicol Sci* **133**, 275-288.

Kirby, M. L. and Waldo, K. L. (1995). Neural Crest and Cardiovascular Patterning. *Circ Res* **77**, 211-215.

Le Douarin, N. M. (2004). The Avian Embryo as a Model to Study the Development of the Neural Crest: A Long and Still Ongoing Story. *Mechanisms of Development* **121**, 1089-1102.

Le Douarin, N. M. K., C (1999). *The Neural Crest.*: Cambridge University Press.

Lee, K. J., Nallathamby, P. D., Browning, L. M., Osgood, C. J. and Xu, X. H. (2007). In Vivo Imaging of Transport and Biocompatibility of Single Silver Nanoparticles in Early Development of Zebrafish Embryos. *ACS Nano* **1**, 133-143.

Martik, M. L. and Bronner, M. E. (2021). Riding the Crest to Get a Head: Neural Crest Evolution in Vertebrates. *Nat Rev Neurosci* **22**, 616-626.

Morris-Kay, G. and Tan, S.-S. (1987). Mapping Cranial Neural Crest Cell Migration Pathways in Mammalian Embryos. *Trends in Genetics* **3**, 257-261.

Nie, J. H., Shen, Y., Roshdy, M., Cheng, X., Wang, G. and Yang, X. (2021). Polystyrene Nanoplastics Exposure Caused Defective Neural Tube Morphogenesis through Caveolae-Mediated Endocytosis and Faulty Apoptosis. *Nanotoxicology* **15**, 885-904.

Nishina, S., Kohsaka, S., Yamaguchi, Y., Handa, H., Kawakami, A., Fujisawa, H. and Azuma, N. (1999). Pax6 Expression in the Developing Human Eye. *Br J Ophthalmol* **83**, 723-727.

Onuma, Y., Takahashi, S., Asashima, M., Kurata, S. and Gehring, W. J. (2002). Conservation of Pax 6 Function and Upstream Activation by Notch Signaling in Eye Development of Frogs and Flies. *Proc Natl Acad Sci USA* **99**, 2020-2025.

Oumer, M., Tazebew, A. and Silamsaw, M. (2021). Birth Prevalence of Neural Tube Defects and Associated Risk Factors in Africa: A Systematic Review and Meta-Analysis. *BMC Pediatr* **21**, 190.

Poelmann, R. E., Gittenberger-de Groot, A. C., Biermans, M. W. M., Dolfing, A. I., Jagessar, A., van Hattum, S., Hoogenboom, A., Wisse, L. J., Vicente-Steijn, R., de Bakker, M. A. G., et al. (2017). Outflow Tract Septation and the Aortic Arch System in Reptiles: Lessons for Understanding the Mammalian Heart. *Evodevo* **8**, 9.

Qiao, J., Chen, R., Wang, M., Bai, R., Cui, X., Liu, Y., Wu, C. and Chen, C. (2021). Perturbation of Gut Microbiota Plays an Important Role in Micro/Nanoplastics-Induced Gut Barrier Dysfunction. *Nanoscale* **13**, 8806-8816.

Rocha, M., Beiriger, A., Kushkowski, E. E., Miyashita, T., Singh, N., Venkataraman, V. and Prince, V. E. (2020). From Head to Tail: Regionalization of the Neural Crest. *Development* **147**, dev193888.

Sana, S. S., Dogiparthi, L. K., Gangadhar, L., Chakravorty, A. and Abhishek, N. (2020). Effects of Microplastics and Nanoplastics on Marine Environment and Human Health. *Environ Sci Pollut Res Int* **27**, 44743-44756.

Santagati, F. and Rijli, F. M. (2003). Cranial Neural Crest and the Building of the Vertebrate Head. *Nat Rev Neurosci* **4**, 806-818.

Schoenwolf, G. C. (2018). Contributions of the Chick Embryo and Experimental Embryology to Understanding the Cellular Mechanisms of Neurulation. *Int J Dev Biol* **62**, 49-55.

Schoenwolf, G. C. and Smith, J. L. (1990). Mechanisms of Neurulation: Traditional Viewpoint and Recent Advances. *Development* **109**, 243-270.

Schoenwolf, G. C. and Smith, J. L. (2000). Mechanisms of Neurulation. *Developmental Biology Protocols: Volume II*, 125-134.

Shimokita, E. and Takahashi, Y. (2011). Secondary Neurulation: Fate-Mapping and Gene Manipulation of the Neural Tube in Tail Bud. *Dev Growth Differ* **53**, 401-410.

Shook, D. and Keller, R. (2003). Mechanisms, Mechanics and Function of Epithelial–Mesenchymal Transitions in Early Development. *Mechanisms of Development* **120**, 1351-1383.

Smits-van Prooije, A. E., Poelmann, R. E., Gesink, A. F., van Groeningen, M. J. and Vermeij-Keers, C. (1986). The Cell Surface Coat in Neurulating Mouse and Rat Embryos, Studied with Lectins. *Anat Embryol (Berl)* **175**, 111-117.

van der Spuy, M., Wang, J. X., Kociszewska, D. and White, M. D. (2023). The Cellular Dynamics of Neural Tube Formation. *Biochem Soc Trans* **51**, 343-352.

Waldo, K., Zdanowicz, M., Burch, J., Kumiski, D. H., Stadt, H. A., Godt, R. E., Creazzo, T. L. and Kirby, M. L. (1999). A Novel Role for Cardiac Neural Crest in Heart Development. *J Clin Invest* **103**, 1499-1507.

Wang, M., Rucklin, M., Poelmann, R. E., de Mooij, C. L., Fokkema, M., Lamers, G. E. M., de Bakker, M. A. G., Chin, E., Bakos, L. J., Marone, F., et al. (2023). Nanoplastics Causes Extensive Congenital Malformations During Embryonic Development by Passively Targeting Neural Crest Cells. *Environ Int* **173**, 107865.

Wang, W. D., Melville, D. B., Montero-Balaguer, M., Hatzopoulos, A. K. and Knapik, E. W. (2011). Tfap2a and Foxd3 Regulate Early Steps in the Development of the Neural Crest Progenitor Population. *Dev Biol* **360**, 173-185.

Wang, X. Y., Li, S., Wang, G., Ma, Z. L., Chuai, M., Cao, L. and Yang, X. (2015). High Glucose Environment Inhibits Cranial Neural Crest Survival by Activating Excessive Autophagy in the Chick Embryo. *Sci Rep* **5**, 18321.

Wilkinson, D. G. (1998). *In Situ Hybridization: A Practical Approach.*: OUP Oxford.

Yan, Y., Wang, G., Huang, J., Zhang, Y., Cheng, X., Chuai, M., Brand-Saberi, B., Chen, G., Jiang, X. and Yang, X. (2020). Zinc Oxide Nanoparticles Exposure-Induced Oxidative Stress Restricts Cranial Neural Crest Development During Chicken Embryogenesis. *Ecotoxicol Environ Saf* **194**, 110415.

Supporting Information

File S1. Supplementary Figure. LB Agar plates tests of PS-NP sterility.

File S2. Statistical analysis of malformation and mortality data on size response.

File S3. Statistical analysis of malformation and mortality data on dose response.

Movies S1. Control chicken embryo, exposed at stage 8 to vehicle only (Ringer's solution), and imaged with MicroCT at 24 hpe.

(Link: https://www.sciencedirect.com/science/article/pii/S0160412023001381r exposure; rotating view.)

Movies S2. Experimental (treated) chicken embryo, exposed at stage 8 to 50 of 25 nm PS-NPS, 5 mg/mL, and imaged with MicroCT 24 h after exposure; rotating view.

(Link: https://www.sciencedirect.com/science/article/pii/S0160412023001381)

Movies S3. Another experimental (treated) chicken embryo imaged with MicroCT.

(Link: https://www.sciencedirect.com/science/article/pii/S0160412023001381)

Table S1. Table of malformations that have been seen at 24 hpe.

Table S2. Table of malformations that have been seen at 4 dpe.

Table S3. Table of malformations that have been seen at 8 dpe.

Table S4. Primers used for PCR.

Fig. S1. Bright field microscopic images of 2 d chicken embryo neural crest cultures 1 h after exposure to PS-NPs (0.1 mg/mL) in culture medium or culture medium only (controls).

File S1. LB Agar plate streaking to confirm the sterility of PS-NPs used in this study. No colonies were observed in any of the plates after overnight incubation at 37 °C. (**a**) 25 nm plain nanoplastics, (**b**) 100 nm plain nanoplastics, (**c**) 500 nm plain nanoplastics.

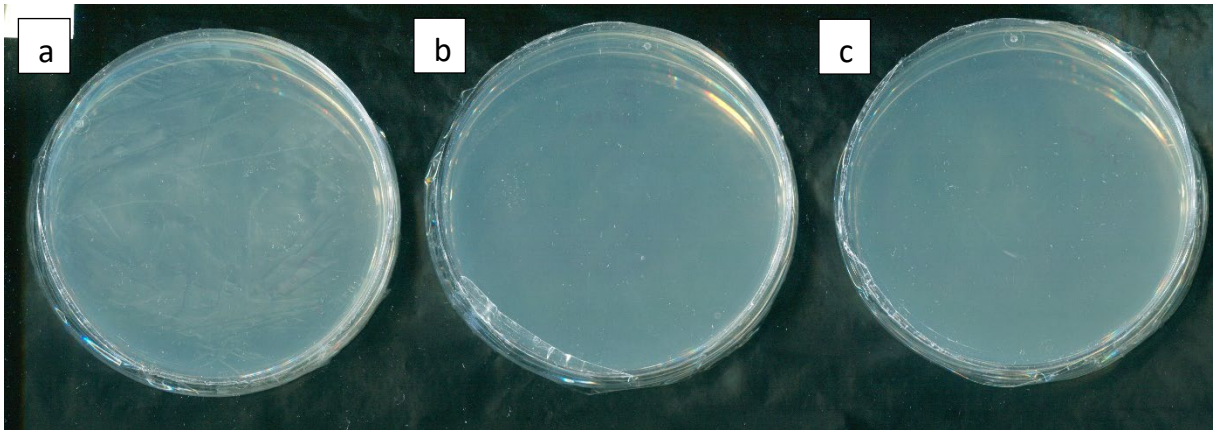

File S2. **Statistical analysis of malformation and mortality data on size response.**

Effects of Polystyrene Size

Method

All computations were performed in **R** version 4.1.3 (R Core Team, 2021). We computed the relative amount of particles as $100 \times \frac{\text{concentration}}{\text{particle size}}$.

We computed χ^2 tests from 2x2 contingency tables to evaluate the difference in death and malformedness between zero and non-zero size, relative amount and concentration of particles. We computed p-values based on both the asymptotic distribution of χ^2 statistics, as well as on Monte Carlo simulation with 2000 simulation replications (Hope, 1968).

Results

The raw data are depicted in Figure 1, where outcomes are plotted against particle size, and Figure 2, where outcomes are plotted against the relative amount of particles. For particle size, we observe highest probabilities of malformedness and death for size 25 nm. There is also a clear increasing probability of malformedness and death if the amount of particles increases. The increasing probability of malformedness and death could be a combined effect of particle size and/or the amount of particles, which cannot be disentangled in the current experiments: Because concentration was kept constant, the amount of particles automatically decreases if particle size increases.

Figure 1

Observed proportions of death and malformedness as a function of particle size.

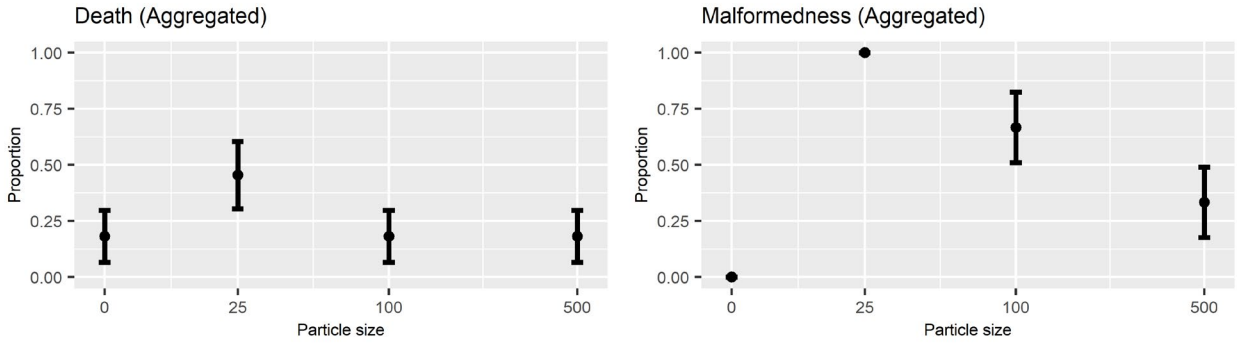

Note. Error bars represent estimated proportions $\pm$ 1 standard error, computed as $\sqrt{\frac{\hat{p}(1-\hat{p})}{n}}$.

Figure 2

Observed proportions of death and malformedness as a function of relative amount of particles.

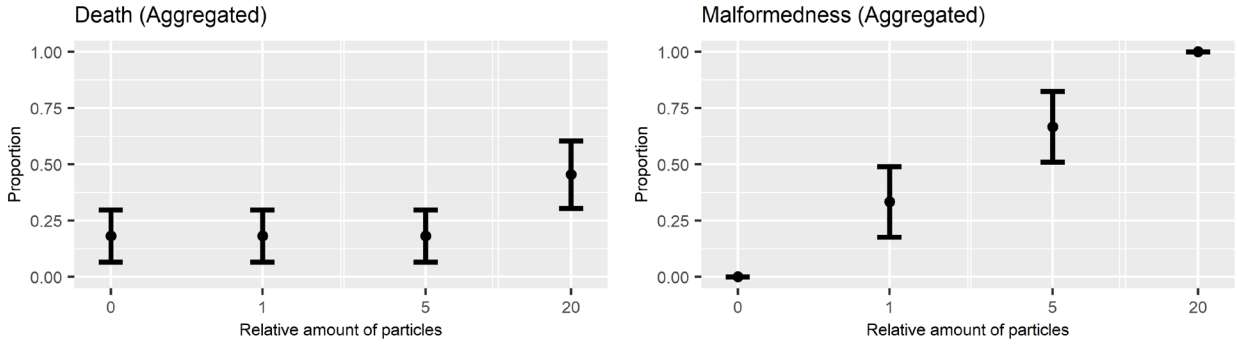

Note. Error bars represent estimated proportions $\pm$ 1 standard error, computed as $\sqrt{\frac{\hat{p}(1-\hat{p})}{n}}$.

We ran χ^2 tests to compare rates of malformedness and death between zero and non-zero particle sizes (with zero particle size equaling a relative amount of zero). χ^2 tests indicated a significant effect of particle size on the probability of malformedness: $X^2(1) = 7.946$; $p = 0.005$; Monte-Carlo $X^2 = 10.313$; $p = 0.003$. No significant effect of particle size on the probability of death was found: $X^2(1) = 0.04$; $p = 0.841$; Monte-Carlo $X^2 = 0.364$; $p = 0.688$.

Raw data

Table 1 presents the raw data on which these analyses were based.

Table 1

Raw data from the experiments.

experiment	size	concentration	relative amount	# normal	# malformed	# dead	# alive	# total	prop. dead	prop. malformed
size	0	0	0	9	0	2	9	11	0.182	0.000
size	25	5	20	0	6	5	6	11	0.455	1.000
size	100	5	5	3	6	2	9	11	0.182	0.667
size	500	5	1	6	3	2	9	11	0.182	0.333

References

Hope, A. C. (1968). A simplified monte carlo significance test procedure. *Journal of the Royal Statistical Society: Series B (Methodological)*, *30*(3), 582–598. https://doi.org/10.1111/j.2517-6161.1968.tb00759.x

R Core Team. (2021). *R: A language and environment for statistical computing*. R Foundation for Statistical Computing. https://www.R-project.org/

File S3. **Statistical analysis of malformation and mortality data on dose response.**

Effects of Polystyrene Concentration

Method

All computations were performed in **R** [version 4.1.3; R Core Team (2021)], using package **drc** [version 3.0.1; Ritz et al. (2015)].

We first computed χ^2 tests from 2x2 contingency tables to evaluate the difference in death and malfermedness between zero and non-zero size, relative amount and concentration of particles. We computed p-values based on both the asymptotic distribution of χ^2 statistics, as well as on Monte Carlo simulation with 2000 simulation replications (Hope, 1968).

We fitted dose-response curves using package **drc** (Ritz et al., 2015), which estimates log-logistic models (i.e., a logistic model with a parameter-dependent link function) using maximum likelihood. We used the 2- and 4-parameter models:

$$f(x) = c + \frac{d - c}{1 + \exp(b(\log(x) - \log(e)))}$$

where x is the dose and $f(x)$ gives the predicted probability of death. Parameter b reflects the effect of dose on the response, with a negative value indicating a positive effect (on death or malformedness, in the current study). Parameter c is a lower limit, and parameter d is an upper limit, both of which can be freely estimated, or fixed to a-priori known constants. If c is fixed to a value of zero and d is fixed to a value of 1, they can be dropped from the equation which yields the 2-parameter model:

$$f(x) = \frac{1}{1 + \exp(b(\log(x) - \log(e)))}$$

To evaluate model fit, we used a Pearson χ^2 goodness-of-fit test, and interpreted a high p-value to indicate acceptable model fit.

Results

Figure 1

Observed proportions of death and malformedness as a function of particle concentration.

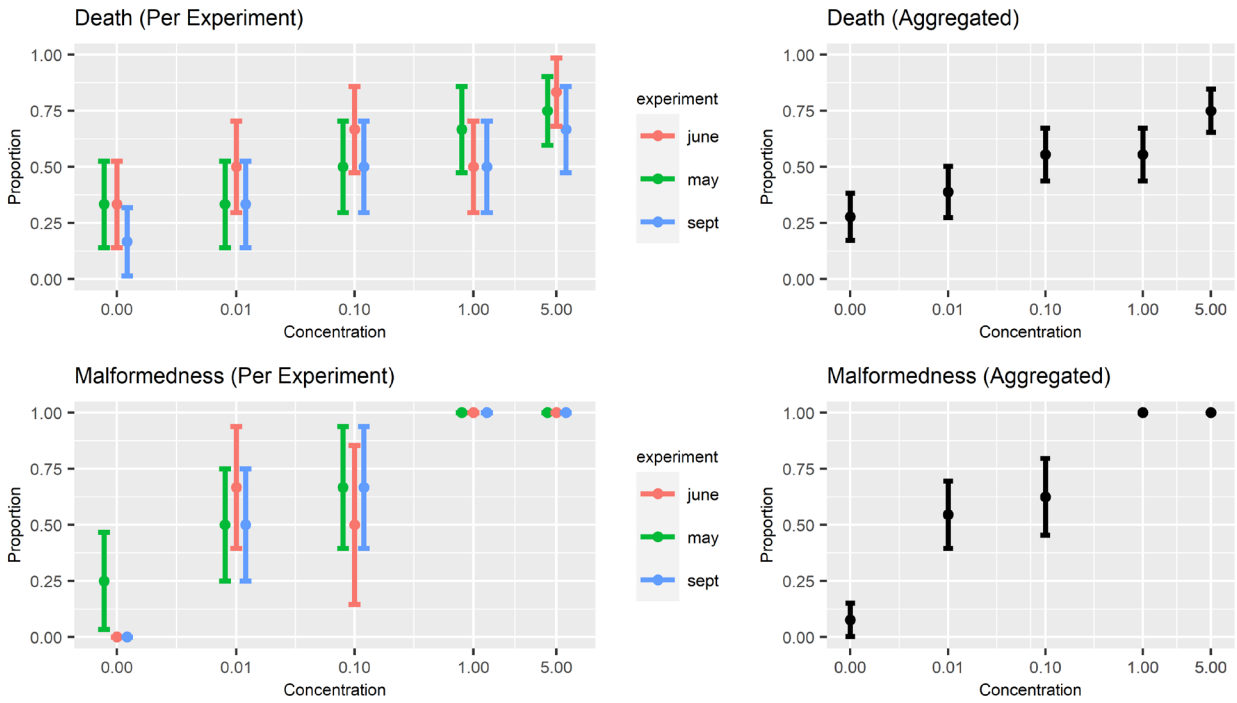

Note. Error bars represent estimated proportions $\pm$ 1 standard error, computed as $\sqrt{\frac{\hat{p}(1-\hat{p})}{n}}$.

The raw data are depicted in Figure 1, where outcomes are plotted against the concentration of particles. The plots indicate an increasing probability of malformedness and death if concentration increases.

We ran χ^2 tests to compare rates of malformedness and death between zero and non-zero concentrations. The χ^2 tests indicated a significant effect of concentration on the probability of malformedness: $X^2(1) = 14.345$; $p < 0.001$; Monte-Carlo $X^2 = 16.962$; $p < 0.001$. The χ^2 tests indicated a significant effect of concentration on the probability of death only according to the Monte-Carlo test: $X^2(1) = 3.775$; $p = 0.052$; Monte-Carlo $X^2 = 4.866$; $p = 0.036$.

Table 1

Parameter estimates for the effect of concentration on malformedness.

	Estimate	Std. error	t-value	p-value
b	-0.606	0.268	-2.261	0.024
e	0.011	0.010	1.088	0.276

Figure 2

Fitted dose-response curve for the effect of concentration on malformedness (2-parameter log-logistic model).

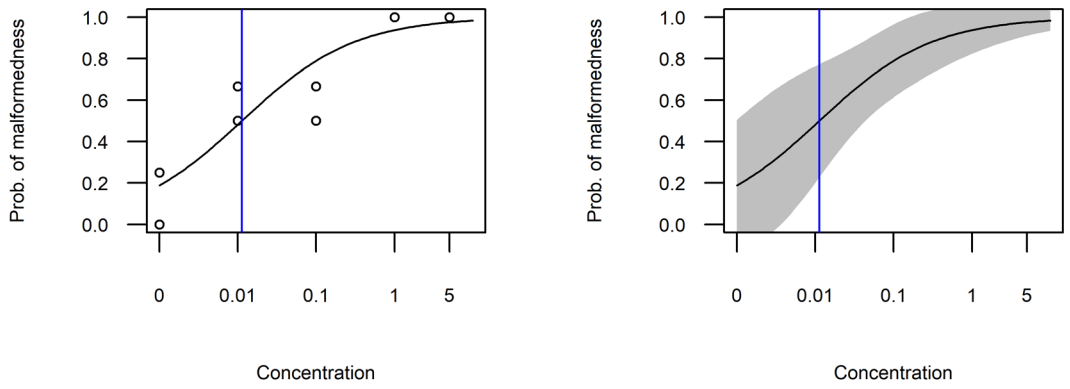

Note. The left plot shows observed datapoints, indicated by dots. The right plot depicts a 95% confidence interval. Blue vertical lines indicate the estimated concentration which would lead to malformedness in 50% of the population.

Next we fitted log-logistic models. Figure 1 indicated that the lower limit of the probability of malformedness is equal to zero, and the upper limit is equal to 1; we thus fitted a 2-parameter log-logistic model for malformedness. Table 1 shows the resulting parameter estimates; the negative and significant value of b indicates a significant effect of concentration on malformedness. Figure 2 shows the fitted dose-response curve. The model showed acceptable model fit: $X^2(10) = 2.63$: $p = 0.989$.

Table 2

Parameter estimates for the effect of concentration on death.

	Estimate	Std. error	t-value	p-value
b	-0.338	0.286	-1.180	0.238
c	0.276	0.104	2.648	0.008
d	0.949	0.553	1.715	0.086
e	0.721	3.781	0.191	0.849

Figure 3

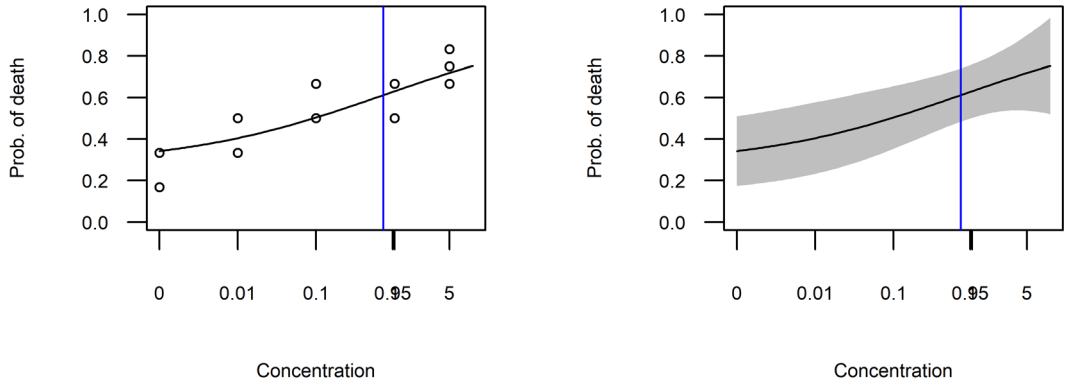

Fitted dose-response curve for the effect of concentration on death (4-parameter log-logistic model).

Note. The left plot shows observed datapoints, indicated by dots. The right plot depicts a 95% confidence interval. Blue vertical lines indicate the estimated LD50.

Figure 3 suggested the lower and upper limits on the probability of death were not equal to 0 and 1, respectively. We fitted a 4-parameter log-logistic model, in which the lower and upper limits are freely estimated; parameter estimates are presented in Table 2. The model showed acceptable model fit: $X^2(11) = 3.097$: $p = 0.989$. The

fitted dose-response curve is depicted in Figure 3. We performed a likelihood ratio test, which tests the null hypothesis of no effect against the 4-parameter dose-response model, which indicated a significant effect of concentration on death: $X^2(3) = 9.476$; $p = 0.024$

Raw data

Table 6 presents the raw data on which these analyses were based.

Table

Raw data from the experiments.

	experiment	size	concentration	# normal	# malformed	# dead	# alive	# total	prop. dead	prop. malformed
5	may	0	0.00	3	1	2	4	6	0.333	0.250
6	may	25	0.04	2	2	2	4	6	0.333	0.500
7	may	25	0.40	1	2	3	3	6	0.500	0.667
8	may	25	4.00	0	2	4	2	6	0.667	1.000
9	may	25	20.00	0	2	6	2	8	0.750	1.000
10	june	0	0.00	4	0	2	4	6	0.333	0.000
11	june	25	0.04	1	2	3	3	6	0.500	0.667
12	june	25	0.40	1	1	4	2	6	0.667	0.500
13	june	25	4.00	0	3	3	3	6	0.500	1.000
14	june	25	20.00	0	1	5	1	6	0.833	1.000
15	sept	0	0.00	5	0	1	5	6	0.167	0.000
16	sept	25	0.04	2	2	2	4	6	0.333	0.500
17	sept	25	0.40	1	2	3	3	6	0.500	0.667
18	sept	25	4.00	0	3	3	3	6	0.500	1.000
19	sept	25	20.00	0	2	4	2	6	0.667	1.000

References

Hope, A. C. (1968). A simplified monte carlo significance test procedure. *Journal of the Royal Statistical Society: Series B (Methodological)*, *30*(3), 582–598. https://doi.org/10.1111/j.2517-6161.1968.tb00759.x

R Core Team. (2021). *R: A language and environment for statistical computing*. R Foundation for Statistical Computing. https://www.R-project.org/

Ritz, C., Baty, F., Streibig, J. C., & Gerhard, D. (2015). Dose-response analysis using R. *PLOS ONE*, *10*(e0146021, 12). https://doi.org/10.1371/journal.pone.0146021

Table S1. **Table of malformations that have been seen at 24 hpe.**

Embryos analysed for phenotypic effects 28 h after treatment with 5mg/mL plain PS-NPs. In the column 'Concentration PS-NPs', 0 mg/mL = Ringer's only controls. HH, Hamburger & Hamilton, 1951 stages.

Embryo number	Concentration of PS-NPs (mg/ml)	Mortality: alive, 0; dead, 1	Gross assessment of phenotype: normal, 0; abnormal, 1	No. somite pairs	Stage (HH)	Phenotype judgement Normal(0)/Abnormal(1)	Neural tube defect location		
							head	trunk	caudal
1	5	1	1						
2	5	0	1	7	9	1	1	1	1
3	5	1	1						
4	5	0	1	13	11	1	1	1	
5	5	1	1						
6	5	0	1	12	11	1	1	1	1
7	5	1	1						
8	5	1	1						
9	5	1	1						
10	5	0	1	13	11	1	1	1	
11	0	1							
12	0	0	0	25	15	0			
13	0	0	0	26	15	0			
14	0	0	0	23	15	0			
15	0	0	0	22	14	0			
16	0	0	0	22	14	0			
17	0	0	0	24	15	0			
18	0	0	0	22	14	0			
19	0	0	0	26	15	0			
20	0	1							
21	5	1							
22	5	0	1	13	11	1	1	1	1
23	5	1							
24	5	0	1	22	14	1	1		
25	5	1							
26	5	0	1			1	1		
27	5	1							
28	5	0	1	n.d	11	1	1	1	1
29	5	1							
30	5	1							

31	0	0	0	19	13				
32	0	1							
33	0	0	0	20	13				
34	0	1							
35	0	0	0	19	13				
36	0	0	0	22	14				
37	0	0	0	17	12				
38	0	0	0	19	13				
39	0	0	0	22	14				
40	0	0	0	20	13				
41	5	0	1	20	13	1		1	
42	5	1							
43	5	1							
44	5	0	1	18	12	1		1	
45	5	0	1	16	12	1	1	1	1
46	5	0	1	15	11	1	1	1	
47	5	0	1	18	12	1	1	1	
48	5	1							
49	5	1							
50	5	1							
51	0	0	0	25	15				
52	0	0	0	22	14				
53	0	0	0	22	14				
54	0	0	0	17	12				
55	0	0	0	22	14				
56	0	0	0	21	13				
57	0	1							
58	0	0	0	15	11				
59	0	1							
60	0	0	0	20	13				
61	5	0	1	18	12	1	1	1	
62	5	0	1	16	12	1	1	1	1
63	5	1							
64	5	1							
65	5	1							
66	5	0	1	17	12	0			
67	5	0	1	17	12	0			
68	5	0	1	19	13	1	1	1	
69	5	0	1	18	12	1		1	
70	5	1							
71	0	0	0	22	14	0			

72	0	0	0	24	15	0			
73	0	1							
74	0	0	0	21	13	0			
75	0	0	0	20	13	0			
76	0	0	0	20	13	0			
77	0	0	0	21	13	0			
78	0	0	0	22	14	0			
79	0	0	0	21	13	0			
80	0	0	0	23	14	0			
81	5	0	1	20	13	0	0	0	0
82	5	1							
83	5	1							
84	5	0	1	18	12	1			1
85	5	1							
86	5	1							
87	5	0	1	20	13	1	1		
88	5	0	0	21	13	1	1		
89	5	0	1	17	12	1	0	1	0
90	5	0	1	17	12	1	1		1
91	0	0	0	20	13	0			
92	0	0	0	20	13	0			
93	0	1							
94	0	0	0	20	13	0			
95	0	0	0	22	14	0			
96	0	0	0	25	15	0			
97	0	0	0	23	14	0			
98	0	0	0	20	13	0			
99	0	0	0	22	14	0			
100	0	0	0	22	14	0			

Table S2. **Table of malformations that have been seen at 4 dpe.**

Embryos analysed for phenotypic effects 4 d after treatment with 5mg/mL plain PS-NPs. In the column 'Concentration PS-NPs', 0 mg/ml = Ringer's only controls.

Embryo number	Concentration of PS-NPs (mg/ml)	Mortality: alive, 0; dead, 1	gross assessment of phenotype: normal, 0; abnormal, 1	Neural tube defect			tail	microphthalmia		
				head	trunk	caudal		left eye	right eye	torsion /flexure
1	0	0	0							
2	0	1								
3	0	0	0							
4	0	0	0							
5	0	1								
6	0	0	1	0						1
7	0.01	0	0							
8	0.01	0	1			1	1			
9	0.01	1								
10	0.01	0	0							
11	0.01	1								
12	0.01	0	1	1		1				1
13	0.1	0	0							
14	0.1	1								
15	0.1	0	1	1		1	1	1		
16	0.1	0	1	1		1	1	1	1	1
17	0.1	1								
18	0.1	1								
19	1	1								
20	1	0	1			1		1	1	
21	1	1								
22	1	1								
23	1	0	1			1				1
24	1	1								
25	5	0	1	1						1

26	5	1									
27	5	1									
28	5	1									
29	5	1									
30	5	0	1			1					1
31	5	1									
32	5	1	0								
33	0	0	0								
34	0	1									
35	0	0	0								
36	0	1									
37	0	0	0								
38	0	0	0								
39	0.01	1									
40	0.01	1									
41	0.01	1									
42	0.01	0	1					1			
43	0.01	0	1						1	1	1
44	0.01	0	0								
45	0.1	0	0								1
46	0.1	0	0								
47	0.1	1									
48	0.1	1									
49	0.1	1									
50	0.1	1									
51	1	0	1	1						1	
52	1	1									
53	1	0									
54	1	1									
55	1	0	1	1	1	1	1	1	1	1	
56	1	1									
57	5	1									
58	5	1									
59	5	0	1	1							1
60	5	1									
61	5	1									
62	5	1									
63	0	1									
64	0	0	1	1							
65	0	0	0								
66	0	0	0								

67	0	0	0						
68	0	0	0						
69	0.01	1							
70	0.01	1							
71	0.01	0	0						
72	0.01	0	1						1
73	0.01	0							
74	0.01	0	1						1
75	0.1	1							
76	0.1	1							
77	0.1	0	1						1
78	0.1	0							
79	0.1	1							
80	0.1	0	1	1					
81	1	1							
82	1	0	1						1
83	1	0	1					1	1
84	1	0	1						1
85	1	1							
86	1	1							
87	5	0	1	1					1
88	5	1							
89	5	1							
90	5	1							
91	5	1							
92	5	0	1	1	1	1	1		

Table S3. **Table of malformations seen at 8 dpe.**

				Neural tube defect			Microphthalmia		Cardiac Malformations (normal,0; abnormal,1)								Comments
Embryo number	**Concentration of PS-NPs (mg/mL)**	**Analysis approach**	**gross assessment of phenotype: normal, 0; abnormal, 1**	**Head**	**Trunk**	**Tail**	**Left**	**Right**	**Craniofacial dysplasia (CD), Cleft Primary Palate (CPP)**	**Vertebral/Axial malformations**	**Failure of ventral side closure**	**Thymic disruption**	**Ventricular septal defect**	**Abnormal pharyngeal arch arteries**	**Persistent truncus arteriosus**	**Aortopulmonary Septal Defect**	
1	0	Alcian blue, H&E	0	0	0	0	0	0	0	0	0	0	0	0	0	0	
2	0	Alcian blue, H&E	0	0	0	0	0	0	0	0	0	0	0	0	0	0	
3	0	Alcian blue, H&E	0	0	0	0	0	0	0	0	0	0	0	0	0	0	
4	0	Alcian blue, H&E	0	0	0	0	0	0	0	0	0	0	0	0	0	0	
5	5	Alcian blue, H&E	1	1	0	n.d	1	1	1(CD)	1	1	1	n,d	n.d	1	n.d	Sample was destroyed while embedding
6	5	Alcian blue, H&E	1	1	1	n.d	0	1	1(CPP)	1	1	1	0	1 (persistent pharyngeal	0	0	Persist 4th arch

													arch artery)				
7	5	Alcian blue, H&E	1	0	0	n.d	0	0	0	1	0	1	1(DORV)	0	0	1	Significant pericardial blebbing, OFTs fail to spiral, common IFT complex
8	5	Alcian blue	1	1	1	n.d	1	1	1(CPP)	1	1	n.d	n.d	n.d	n.d	n.d	Phocomelia and severe microphthalmia
9	5	Alcian blue	1	1	1	n.d	1	1	1(CD)	1	1	n.d	n.d	n.d	n.d	n.d	
10	5	Alcian blue	1	1	n.d	n.d	0	1	1(CD+CPP)	1	1	n.d	n.d	n.d	n.d	n.d	severe facial clefting
11	0	Synchrotron	0	0	0	0	0	0	0	0	0	0	0	0	0	0	
12	5	Synchrotron	1	n.d	n.d	n.d	n.d	n.d	n.d	n.d	n.d	n.d	1	1(2 extra pharyngeal arch arteries)	0	0	
13	5	Synchrotron	1	n.d	n.d	n.d	n.d	n.d	n.d	n.d	n.d	n.d	1	0	0	1	Pericardial blebbing
14	0	Synchrotron	0	0	0	0	0	0	0	0	0	0	0	0	0	0	
15	5	Synchrotron	1	n.d	n.d	n.d	n.d	n.d	n.d	n.d	n.d	n.d	0	0	0	0	
16	5	Synchrotron	1	n.d	n.d	n.d	n.d	n.d	n.d	n.d	n.d	n.d	0	0	0	0	

Table S4. **Primers used for PCR.**

Gene	Forward Primers	Reverse Primer	Accession NCBI Reference Sequence
FOXD3 (Forkhead box D3)	CGAAGAGCAGCCTGGTGAAGC	CGATGATGTTGGTAGGCACGCT	NM_204951.3
SNAI2 (Snail family transcriptional repressor 2)	CCACGCTCCTTCCTGGTC	CCAGGTAAACATTGACTGCATGA	CR407272
WNT1(Wnt family member 1)	TCTGATCCGACAGAACCCCG	GTCCCCATCTTCCCGCTGTA	NM_001396681.1
SOX10 (SRY-box 10)	GCAGCCTTCACAGGGTTTG	CCCTTCTCGCTTGGAGTCAG	NM_204792.2
LMO4 (LIM domain only 4)	CTACACCAAGAGCGGCATGA	AGTCTCCCATTAGCCCAGGT	NM_204112.2
PAX3 (Paired box 3)	TCGGGAAGAACTCGCACAAA	GCGAGACCGGAAAATAACACC	NM_001397759.1
TFAP2A (Transcription factor AP-2 alpha)	CCAAGTCTAACAACAACGCC	TTTCGGTGCTTCTCCTCTTT	NM_205094.2

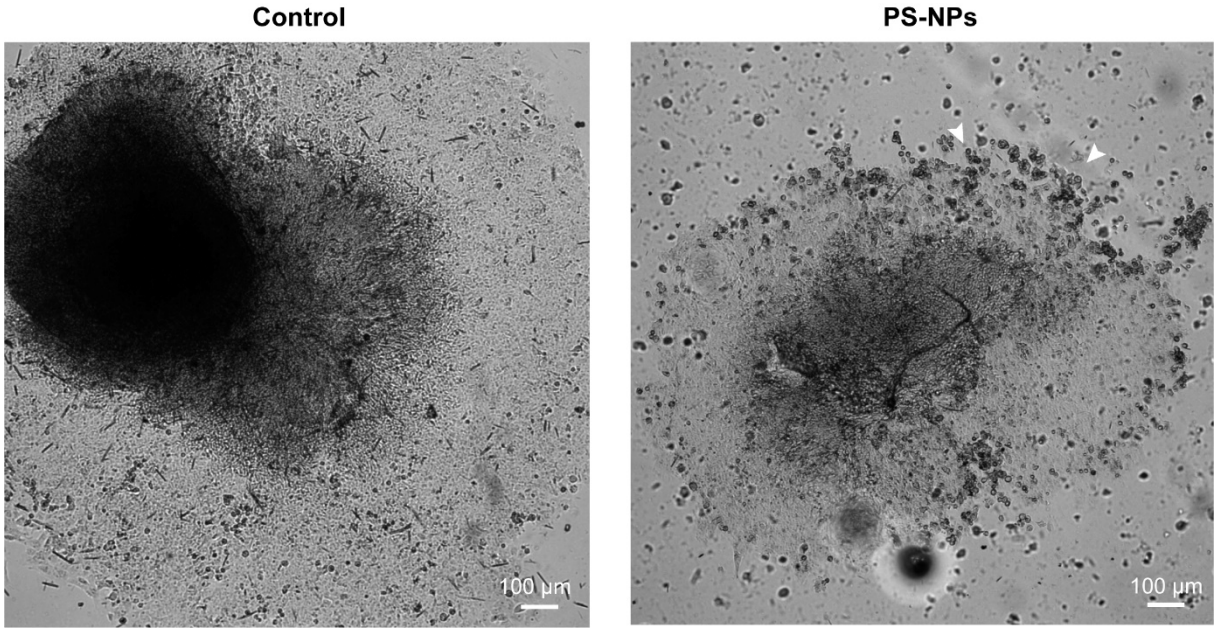

Fig. S1. Bright field microscopic images of 2 d chicken embryo neural crest cultures 1 h after exposure to PS-NPs (0.1 mg/mL) in culture medium or culture medium only (controls). Note the dead cells (white arrowheads) in the PS-NP treated culture.